

UniRestorer: Universal Image Restoration via Adaptively Estimating Image Degradation at Proper Granularity

Jingbo Lin¹, Zhilu Zhang¹, Wenbo Li², Renjing Pei², Hang Xu², Hongzhi Zhang¹, Wangmeng Zuo¹
¹Harbin Institute of Technology ²Huawei Noah’s Ark Lab

Abstract

Recently, considerable progress has been made in all-in-one image restoration. Generally, existing methods can be degradation-agnostic or degradation-aware. However, the former are limited in leveraging degradation-specific restoration, and the latter suffer from the inevitable error in degradation estimation. Consequently, the performance of existing methods has a large gap compared to specific single-task models. In this work, we make a step forward in this topic, and present our UniRestorer with improved restoration performance. Specifically, we perform hierarchical clustering on degradation space, and train a multi-granularity mixture-of-experts (MoE) restoration model. Then, UniRestorer adopts both degradation and granularity estimation to adaptively select an appropriate expert for image restoration. In contrast to existing degradation-agnostic and -aware methods, UniRestorer can leverage degradation estimation to benefit degradation-specific restoration, and use granularity estimation to make the model robust to degradation estimation error. Experimental results show that our UniRestorer outperforms state-of-the-art all-in-one methods by a large margin, and is promising in closing the performance gap to specific single-task models. The code and pre-trained models will be publicly released.

1. Introduction

Image restoration is a fundamental task in computer vision, it aims to restore high-quality (HQ) images from corresponding low-quality (LQ) counterparts, including denoising [1, 109], deblurring [64, 73, 110], de-weathering [24, 53, 57, 99], low-light enhancement [86, 92, 111], etc. In the past decade, advanced deep neural architectures [28, 58, 70, 83, 108] have driven image restoration methods to evolve from task-specific [21, 34, 72, 79, 101?] to task-agnostic [16, 48, 51, 97, 98] backbones. Recently, influenced by the success of foundation models in natural language processing and high-level vision, there has been increasing interest in addressing multiple image restoration

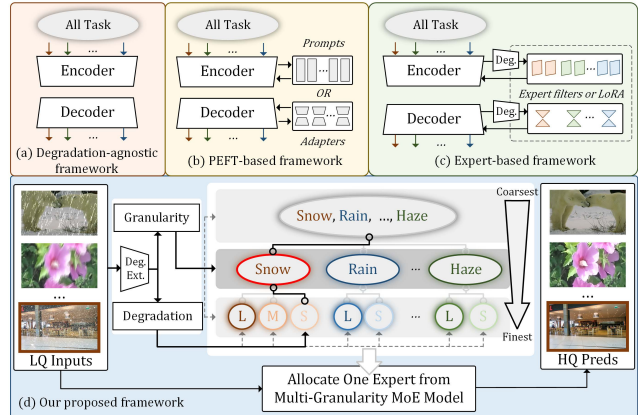


Figure 1. **Illustration of representative all-in-one image restoration frameworks.** (a) Degradation-agnostic methods [85, 103] train a shared backbone using data from all tasks and are limited in leveraging degradation-specific restoration. (b) PEFT-based methods [5, 26, 40, 67, 82, 90, 100] apply learnable prompts or adapters to the backbone to adapt various tasks. (c) Expert-based methods [12, 13, 15, 20, 47, 49, 66, 87, 93, 94, 115] train specific MoE, LoRA, or filters for specific tasks. However, both (b) and (c) suffer from the inevitable error in degradation estimation. (d) We construct a multi-granularity degradation space and a multi-granularity MoE restoration model. By adaptively estimating image degradation at proper granularity, our UniRestorer can be effective in leveraging degradation-specific restoration while being robust to degradation estimation error.

tasks within a single framework, known as all-in-one image restoration [32].

A straightforward approach is to utilize data from all tasks to train a degradation-agnostic model (see Fig. 1 (a)), but it easily yields unsatisfactory results due to the conflicts between certain tasks (e.g., denoising and deblurring). Inspired by parameter-efficient fine-tuning (PEFT) methods [10, 29], learnable prompts [26, 40, 67, 82, 90, 100] and adapters [5] are integrated into the restoration model to modulate intermediate features (see Fig. 1 (b)), allowing the model to process different tasks more specifically. Furthermore, some methods introduce mixture-of-experts (MoE) [13, 15, 47, 87, 94] (MoE-like using filters [12, 20, 49, 66, 93, 115] and low-rank adaptation [3, 81]) modules,

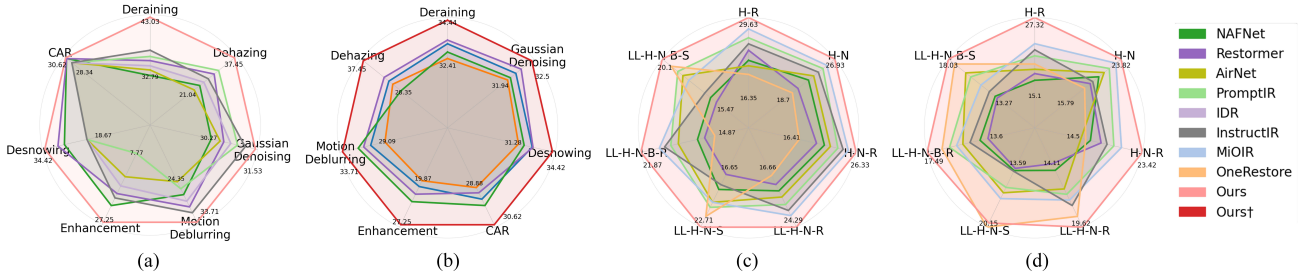


Figure 2. **Comparisons with task-agnostic methods, all-in-one methods, and single-task models.** Ours and Ours[†] denote *auto* and *instruction* modes, which are respectively used for a fair comparison with all-in-one and specific single-task models. **(a)** Comparisons on single-degradation all-in-one setting. **(b)** Comparisons with specific single-task models. **(c)** Comparisons on mixed-degradation all-in-one setting (*in-dist.*). **(d)** Comparisons on mixed-degradation all-in-one setting (*out-dist.*).

routing the current feature to specific experts based on deep features and estimated degradation representations (DRs), as shown in Fig. 1 (c).

Despite rapid progress, these methods show limited performance and fall significantly behind specific single-task models. The degradation-agnostic models cannot leverage the benefits from degradation estimation based priors to improve all-in-one restoration performance. PEFT-based and MoE-based methods provide degradation-aware ways for processing different corruptions specifically conditioning on degradation estimation. However, their performance heavily relies on accurate degradation estimation, which is difficult due to the broad range of degradation space of all-in-one image restoration. Thus, it is inevitable for degradation-aware models suffering from errors in degradation estimation. Inaccurate estimation can cause images to be inappropriately processed by the model, resulting in decreased restoration performance.

From the above analysis, one plausible solution to improve all-in-one restoration is to estimate and leverage image degradation while being robust to degradation estimation error. To achieve this, we propose to first learn DRs in multiple granularities with different fineness (‘ALL’, ‘TYPE’, ‘DEGREE’), and then construct a multi-granularity MoE restoration model corresponding to multi-granularity DRs. Therein, finer experts focus on processing the more specific degradation, *e.g.*, light snow, or heavy snow, thus improving restoration performance significantly; coarser experts have better generalization ability by being trained on wider degradation space. For more robust expert routing, beyond vanilla degradation estimation, we introduce granularity estimation to indicate the degree of degradation estimation error, as illustrated in Fig. 1 (d). Intuitively, given an image with light snow, when the degradation is estimated with large error, the granularity estimation will assign a coarser-grained expert, *e.g.*, a model for general snow, to alleviate the effect of estimation error. When degradation is precisely estimated, granularity estimation will allocate a finer-grained expert, *e.g.*, a model for light snow. Thus, using both degradation and granularity esti-

mation, our method can adaptively allocate the appropriate expert to given unknown corrupted inputs. As a result, our method can effectively utilize image degradation estimation while alleviating the negative effect caused by error-prone degradation estimation.

Specifically, we take the following steps to implement our UniRestorer. First, we optimize a degradation extractor that is aware of finer-grained image degradation. Second, all low-quality images in the training set are fed into the degradation extractor, and their features are then hierarchically clustered into multiple DR groups at different granularities respectively, which forms the multi-granularity degradation set shown in Fig. 3. Third, we train a multi-granularity MoE restoration model based on the constructed multi-granularity degradation set. Fourth, given an image with unknown degradation, we learn routers based on both degradation and granularity estimation results. The router identifies which DR group the degradation and granularity best match in the degradation set, and then allocates the corresponding expert for inference.

To demonstrate the effectiveness and universality of the proposed method, we conduct experiments on both single-degradation and mixed-degradation images. For the single-degradation setting, we unify 7 common image restoration tasks. For the mixed-degradation setting, we introduce 6 degradation types. In addition, we conduct a comprehensive comparative evaluation. The results indicate that our method not only significantly outperforms existing all-in-one methods but also achieves performance that is competitive with, or even superior to, specific single-task models.

The main contributions can be summarized as follows:

- We propose to learn all-in-one image restoration in multiple granularities with different degradation representation fineness (*i.e.*, ‘ALL’, ‘TYPE’, ‘DEGREE’). Specifically, we train a multi-granularity MoE restoration model, which simultaneously maintains superior restoration performance and good generalization ability.
- To alleviate the effect of degradation estimation error on expert routing, we propose to estimate a proper granularity for image degradation. Based on both degradation and

granularity estimation, we can allocate the most appropriate expert for unknown corruptions.

- Extensive experiments conducted on both single-degradation and mixed-degradation images show that our method significantly outperforms existing all-in-one methods and effectively closes the performance gap with specific single-task models.

2. Related Work

Image Restoration for Specific Tasks. Pioneer works propose tailored frameworks for specific degradations, *e.g.*, DnCNN [101] for denoising, SRCNN [21] for super-resolution, DeblurGANv2 [34] for deblurring, PReNet [72] for draining, Dehazformer [79] for dehazing, and DesnowNet [?] for desnowing. Benefits from advanced deep neural networks, some works tend to develop task-agnostic models, such as MPRNet [97], SwinIR [48], NAFNet [16], and Restormer [98], which become strong baselines in various image restoration tasks.

PEFT-based All-in-One Image Restoration. To adapt to various corruptions, pioneer all-in-one image restoration methods [5, 40, 67, 82, 90, 100] integrate PEFT-based techniques [10, 29] and feature modulation [102] into the restoration backbone. For example, TransWeather [82] and AirNet [40] learn degradation-related embeddings as prompts to modulate deep features based on different corrupted inputs. Similarly, PromptIR [67] and IDR [100] employ prompt learning in a more powerful backbone [98] and achieve state-of-the-art performance. MiOIR [90] further exploits the benefits of incorporating explicit prompt and adaptive prompt learning.

Expert-based All-in-One Image Restoration. Mixture-of-Experts (MoE) has proven to be a solution to multi-task learning due to its conditional processing capability [17, 18, 114]. Although prompt learning-based techniques work similarly to MoE in conditional processing, they are still limited in performance and task range. Recent MoE-based all-in-one image restoration methods can be categorized into implicit MoE [12, 20, 93, 94] and explicit MoE [4, 13, 15, 66, 81, 96, 115]. The experts in the former methods are implicitly learned in training and do not correspond to a specific task. Methods belonging to explicit MoE learn experts for specific tasks, unleashing the power of additionally increased parameters. Based on shared backbone, WGWSNet [115] and ADMS [66] learn specific filters for specific tasks. To be more efficient, DaAIR [96], InstructIPT [81], and LoRA-IR [4] learn individual LoRA weights or adapters for each task. By combining knowledge of the shared backbone and task-specific modules, these methods can adapt to different tasks effectively. GRIDS [13] and RestoreAgent [15] divide one complete degradation space into subspaces and learn specific expert full models to alleviate potential conflicts between different degradations.

We have two main advantages compared to previous methods. Most previous methods learn DRs in ‘ALL’ or ‘TYPE’ granularity and generally adopt the error-prone degradation estimation as processing condition. We exploit DRs in multiple granularities, which can be coarse the same as task-agnostic and finer than existing MoE-based methods, thus the learned experts allow for better restoration and generalization performance. In addition, we take into account both the degradation estimation and the estimation error for a more robust routing process.

3. Proposed Method

In this section, we introduce our all-in-one image restoration framework, UniRestorer. We first optimize one degradation representation (DR) extractor that learns DRs at a fine-grained level, *i.e.*, degradation ‘DEGREE’. Based on DRs extracted from all low-quality training data, we conduct hierarchical data clustering that separates DRs into multiple DR groups at different granularities, *i.e.*, ‘ALL’, ‘TYPE’, and ‘DEGREE’ (see Fig. 3), leading to a multi-granularity degradation set and MoE restoration model. To alleviate the inevitable error caused by degradation estimation in routing, we adopt both degradation and granularity estimation to allocate the most appropriate expert to given unknown corrupted inputs.

We first give a preliminary knowledge of the Mixture-of-Experts in Sec. 3.1. In Sec. 3.2, we introduce the training of fine-grained DR extractor, and then provide the hierarchical degradation clustering process to construct a multi-granularity degradation set and MoE restoration model. In Sec. 3.3, we introduce granularity estimation and how to adopt both degradation and granularity estimation for adaptive routing.

3.1. Preliminaries

Mixture-of-Experts [23, 37, 68, 71, 75, 116] is a promising way for scaling up and deploying large or gigantic models due to its competitive computational bounds and latency compared to the vanilla single model. Expert network set $\{\mathcal{F}\}$ and routing network $\mathcal{G}(\cdot)$ are two basic components of MoE architecture. The expert network can be a sub-layer or a sub-network (*e.g.*, convolution layer or feed-forward layer), and it also can be an independently trained network. Given input \mathbf{X} , the routing network $\mathcal{G}(\cdot)$ is used to calculate the contribution of each expert to the final output,

$$y = \sum_{i=0}^N \mathcal{G}(h) \cdot \mathcal{F}_i(\mathbf{X}), \quad (1)$$

where h is commonly a type of representation of input \mathbf{X} which the routing network can assign expert conditioning on. The routing network is typically a noisy top-k routing network parameterized with w_g and w_n , which models $P(\mathcal{F}_k|h)$ as the probability of using the k -th expert \mathcal{F}_k and

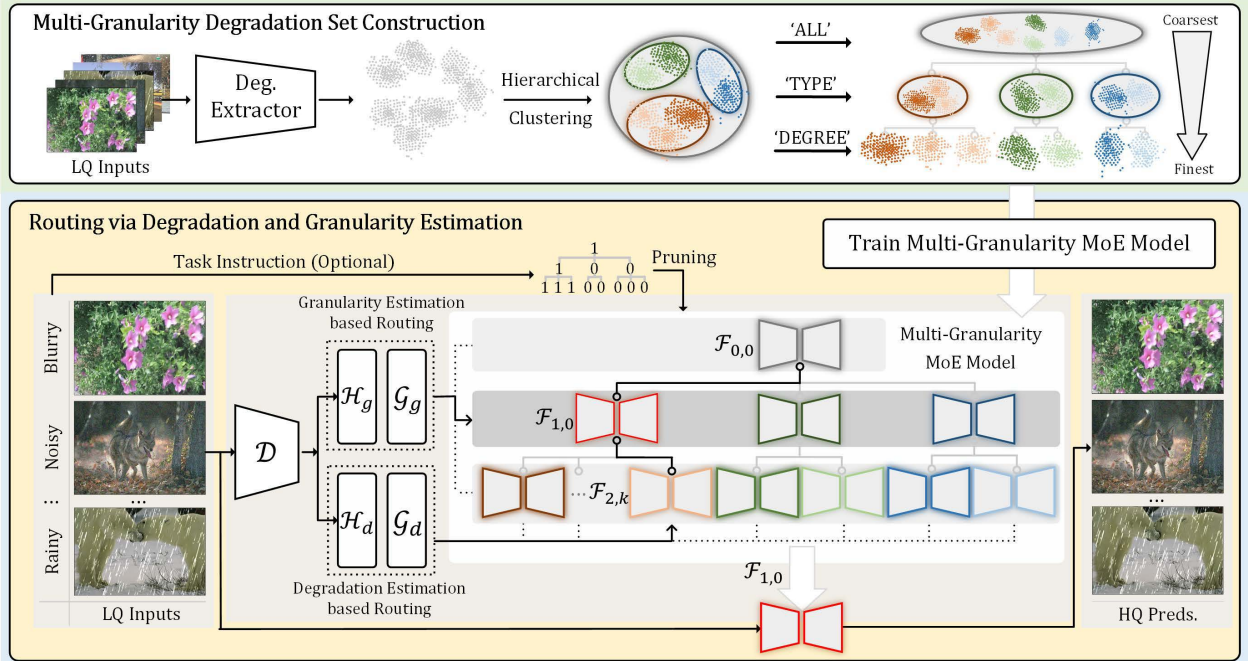


Figure 3. **Illustration of our proposed UniRestorer.** We develop a multi-granularity degradation set by hierarchical clustering on extracted DRs at different granularity, *i.e.*, ‘ALL’, ‘TYPE’, and ‘DEGREE’. Based on the multi-granularity degradation set, we train a multi-granularity MoE restoration model. Besides vanilla degradation estimation, we introduce granularity estimation to indicate the degree of degradation estimation error. Adopting both degradation and granularity estimation, we train routers to adaptively allocate an expert to unknown corrupted input.

selects experts with top- k probability to contribute to the final output. The noisy routing process can be described as follows,

$$\mathcal{G}(h) = \text{Softmax}(h \cdot w_g) + \mathcal{N}(0, 1) \text{Softplus}(h \cdot w_n), \quad (2)$$

where Softplus is the smooth approximation to the function ReLU . Then, the $\text{TopK}(\cdot, k)$ function is used to select the experts with the largest k values according to $\mathcal{G}(h)$.

3.2. Multi-Granularity Degradation and Expert

Fine-Grained DR Extractor. Considering the convenience of using text to represent the type of degradation on corrupted images, we adopt a CLIP-based method, DA-CLIP [59], as our basic backbone. Using contrastive learning, DA-CLIP trains an image controller to separate different corrupted inputs. However, aiming to exploit finer-grained DRs (*i.e.*, degradation degree), it is essential to enable the DR extractor to be aware of finer-grained representation of degradation. Motivated by the above, we train a fine-grained DR extractor to fit our goal. In our experiments, we found that the estimation of degradation degree is sensitive to distortions, *e.g.*, noise can be heavily alleviated by transformations in the pre-processing of CLIP. To alleviate the effect of distortion on the original degradation, we construct a dataset with fine-grained level degradations. In training, we first crop high-resolution clean images into 224×224 patches and then add synthetic degradations with

different types and degrees to obtain low-quality inputs. During inference, we center-crop the main body of given low-quality inputs to alleviate the influence of the resolution gap between training and inference. Following [59], we employ BLIP [43, 44] to generate captions for clean patches. Thus, the fine-grained DR e can be learned by the DR extractor \mathcal{D} , *i.e.*,

$$e = \mathcal{D}(\mathbf{X}). \quad (3)$$

When training is finished, we employ \mathcal{D} to obtain the DR set $\{e\}$ from all training samples.

Hierarchical Degradation Clustering. To construct the proposed multi-granularity degradation set, we utilize an unsupervised data clustering approach [62], which is simple yet effective. The constructed degradation set is hierarchical. The i -th level of granularity consists of non-overlapped DR groups, each of which is related to a data distribution, and samples drawn from one distribution are with similar DRs. In our implementation, we construct a hierarchical degradation set with n levels of granularities ($n = 3$). The coarsest level is 0-th level and the finest level is n -th level. We first conduct data clustering at the finest-grained level by,

$$\{u\}_n \leftarrow \text{K-means}(\{e\}), \quad (4)$$

where $\{u\}_n$ is the set of cluster centers of the finest-grained level. Based on $\{u\}_n$, we further conduct clustering in coarser-grained levels until the coarsest level. As

a result, we obtain sets of cluster centers of our multi-granularity degradation set in coarse-to-fine level, *i.e.* $\{u\}_0, \{u\}_1, \dots, \{u\}_n$. Then, in the i -th level, we use function $\text{argmin}_{u_{i,j} \in \{u\}_i} (\|e - u_{i,j}\|_2^2)$ to decide which DR group the samples belong to, and thus we can prepare training samples for each expert restoration model $\mathcal{F}_{i,j}$.

Multi-Granularity MoE Restoration Model. We train one multi-granularity MoE restoration model based on obtained multi-granularity degradation set. Expert networks are trained with ℓ_1 loss as the reconstruction loss between predicted results $\hat{\mathbf{Y}}$ and target \mathbf{Y} , *i.e.*,

$$\ell_1 = \|\hat{\mathbf{Y}} - \mathbf{Y}\|_1. \quad (5)$$

Experts trained at coarser-grained levels can generalize to a large range of degradations, and experts trained in finer-grained levels can highly improve the restoration performance on degradations which they are good at. Therefore, given corrupted inputs, we can estimate their DRs and assign them to the most appropriate expert.

3.3. Routing via Degradation and Granularity Est.

It makes sense to use estimated DRs as the routing condition h in Eq. (1). However, degradation estimation is error-prone, which may lead to inaccurate routing and thus impede restoration performance. To this end, based on the constructed multi-granularity degradation set, we estimate image degradation at the proper granularity level, and perform routing based on both degradation and granularity estimation, which makes our method robust to degradation estimation error. We train two separate branches (\mathcal{H}_d and \mathcal{H}_g) upon \mathcal{D} for degradation estimation vector e_{deg} at the finest-grained level and granularity estimation vector e_{gran} . Then, we further train two routers $\mathcal{G}_d(\cdot)$ and $\mathcal{G}_g(\cdot)$ as Eq. (2) based on degradation and granularity estimation, respectively. The routing process can be described as follows,

$$\begin{aligned} \mathcal{F}_{n,k} &= \text{TopK}(\mathcal{G}_d(e_{deg})|\{\mathcal{F}\}_n) \\ \mathcal{F}_{i,j} &= \text{TopK}(\mathcal{G}_g(e_{gran})|\{\mathcal{F}_{0,0}, \dots, \mathcal{F}_{n,k}\}). \end{aligned} \quad (6)$$

\mathcal{G}_d is conducted in the finest-grained level. Based on its routing result, it further selects a set of experts that can solve degradations belonging to DR group $\{e\}_{n,k}$ and are trained in different granularity levels from 0 to n . Furthermore, \mathcal{G}_g is responsible for selecting an expert training in the proper granularity according to granularity estimation.

Inspired by data uncertainty learning [14], we learn e_{deg} and e_{gran} by introducing loss as,

$$\mathcal{L}_{dg} = \frac{1}{2e_{gran}}(u_{y_i} - e_{deg})^2 + \frac{1}{2} \ln e_{gran}, \quad (7)$$

where u_{y_i} is the weight center in the finest-grained level obtained by Eq. (4). We use the first term to build the relationships of e_{deg} and e_{gran} , when the distance between current degradation estimation and corresponding weight center is high, a larger e_{gran} is used to ensure that \mathcal{L}_{dg}

is not too high. Therefore, the granularity can be seen as the degree of the current degradation estimation error. If estimated with a large error, granularity estimation will allocate a coarser-grained expert; Conversely, if degradation estimation is precise, granularity estimation will allocate a finer-grained expert. Thus, conditioning on both e_{deg} and e_{gran} , we can dynamically allocate given corrupted inputs with the most appropriate expert. For stable training, and to avoid the result of \mathcal{G}_g collapse to the finest-grained level, we further adopt load-balance loss as used in [75],

$$\mathcal{L}_{load} = \sigma/\mu, \quad (8)$$

where μ and σ are mean and standard deviation of experts load, respectively. At last, we train our routers by jointly adopting loss as,

$$\mathcal{L}_{total} = \ell_1 + \alpha \mathcal{L}_{dg} + \beta \mathcal{L}_{load}, \quad (9)$$

where α and β are two hyper-parameters to trade-off the effect of \mathcal{L}_{dg} and \mathcal{L}_{load} .

Typically, our framework automatically conducts the processing pipeline of extraction-recognition-routing-restoration (*auto* mode). When users are convinced about the type of degradation, we provide options that users can provide the type of degradation to instruct the routing process (*instruction* mode), as shown in Fig. 3. The instruction plays the role of pruning, it utilizes a set of masks to prune the corresponding DR groups from the multi-granularity degradation set, leading to a more efficient and accurate routing.

4. Experiments

4.1. Experimental Setup

Comparison Settings. We train and evaluate our framework on two all-in-one image restoration settings: (1) **Single-degradation:** we train a universal model to solve 7 image restoration tasks, including deraining (‘R’), dehazing (‘H’), Gaussian color denoising (‘N’), single-image motion deblurring (‘B’), low-light enhancement (‘LL’), denoising (‘S’), and compression artifacts removal (‘J’). We collect data of every included image restoration task and adopt the concatenation of the collected data as training data. (2) **Mixed-degradation:** we develop our experiments in a much more complex degradation space, including 6 types of degradations used in single-degradation, and we evaluate 7 challenging mixed degradation settings, *e.g.*, H-R, H-N, H-N-R, LL-H-N-R, LL-H-N-S, LL-H-N-B-R, and LL-H-N-B-S. To demonstrate the generalization ability, we conduct comparisons on *real-world* degradations and *unseen* degradations, including LHP [25] for real-world deraining, LOLv2 [92] for real-world low-light enhancement, RealSnow [57] for real-world desnowing, RainDrop [69] for raindrop removal, TOLED [113] for under-display camera image restoration, and UIEB [41] for underwater image

Table 1. **All-in-One image restoration (single-degradation) results.** We train task-agnostic models and our method on the concatenation of all restoration training data. The performance of other methods is referred from [20]. n ‘T’ means the average performance of n tasks (3T: Derain, Dehaze, Denoise; 5T: Derain, Dehaze, Denoise, Deblur, Lowlight; 7T: all).

Methods	Derain		Dehaze		Denoise		Deblur		Lowlight		Desnow		CAR		Average		
	Rain100L[95]	SOTS[39]	BSD68[61]	GoPro[64]	LOLv1[86]	Snow100K[57]	LIVE1[76]	3T	5T	7T							
	PSNR	SSIM	PSNR														
MPRNet [97]	25.56	0.903	16.37	0.806	23.92	0.702	25.40	0.858	7.75	0.124	19.33	0.740	27.77	0.889	18.51	22.68	19.66
SwinIR [48]	21.20	0.837	15.94	0.775	24.12	0.780	16.86	0.735	13.80	0.409	18.60	0.718	15.61	0.746	17.55	17.09	18.45
NAFNet [16]	31.32	0.967	22.43	0.907	30.27	0.918	26.53	0.877	<u>23.09</u>	0.796	26.33	0.889	31.26	0.946	24.55	25.76	26.28
Restormer [98]	34.25	0.981	29.64	0.971	31.00	<u>0.929</u>	27.50	<u>0.896</u>	22.80	0.821	<u>28.24</u>	<u>0.914</u>	<u>31.21</u>	<u>0.946</u>	30.46	28.56	<u>28.27</u>
DL [22]	32.62	0.931	26.92	0.391	30.12	0.838	-	-	-	-	-	-	-	-	28.09	-	-
AirNet [40]	34.90	0.967	27.94	0.962	31.06	0.872	-	-	-	-	-	-	-	-	29.29	-	-
PromptIR [67]	36.37	0.972	<u>30.58</u>	<u>0.974</u>	31.12	0.873	-	-	-	-	-	-	-	-	<u>31.50</u>	-	-
InstructIR-3D [20]	<u>37.98</u>	<u>0.978</u>	30.22	0.959	31.32	0.875	-	-	-	-	-	-	-	-	31.49	-	-
DL [22]	21.96	0.762	20.54	0.826	23.09	0.745	19.86	0.672	19.83	0.712	-	-	-	-	21.02	20.28	-
Transweather [82]	29.43	0.905	21.32	0.885	29.00	0.841	25.12	0.757	21.21	0.792	-	-	-	-	23.31	24.41	-
TAPE [52]	29.67	0.904	22.16	0.861	30.18	0.855	24.47	0.763	18.97	0.621	-	-	-	-	24.10	24.28	-
AirNet [40]	32.98	0.951	21.04	0.884	30.91	0.882	24.35	0.781	18.18	0.735	-	-	-	-	23.82	24.10	-
IDR [100]	35.65	0.965	25.20	0.938	31.09	0.883	26.65	0.810	20.70	0.820	-	-	-	-	27.36	26.86	-
InstructIR-5D [20]	36.84	0.973	27.10	0.956	<u>31.40</u>	0.887	<u>29.40</u>	0.886	23.00	<u>0.836</u>	-	-	-	-	28.99	<u>29.19</u>	-
Ours	41.68	0.996	36.44	0.984	31.43	0.936	31.48	0.948	26.67	0.863	31.12	0.940	30.57	0.926	36.71	33.38	31.34

Table 2. **All-in-One image restoration (mixed-degradation) results.** We train task-agnostic methods on synthetic mixed degradation datasets based on DF2K. The performance is evaluated on DIV2K-valid with *in-dist.* and *out-dist.* degradation parameters. ‘ n T’ means the average performance of n tasks (3T: H-R, H-N, H-N-R; 5T: H-R, H-N, H-N-R, LL-H-N-R, LL-H-N-B-R; 7T: all).

Methods	H-R		H-N		H-N-R		LL-H-N-R		LL-H-N-S		LL-H-N-B-R		LL-H-N-B-S		Average		
	PSNR	SSIM	3T	5T	7T												
<i>In-distribution</i>																	
MPRNet [97]	17.22	0.691	19.02	0.717	17.18	0.639	17.25	0.549	17.18	0.583	16.99	0.466	<u>16.80</u>	0.506	17.80	17.57	17.37
SwinIR [48]	16.35	0.620	18.74	0.693	16.48	0.585	16.78	0.513	16.73	0.555	16.54	0.434	16.10	0.482	17.19	17.01	16.81
NAFNet [16]	19.14	0.775	22.71	0.843	18.56	0.723	17.41	0.603	17.09	0.631	16.37	0.505	15.83	<u>0.530</u>	20.13	18.98	18.15
Restormer [98]	19.85	0.795	20.44	0.820	17.64	0.719	16.86	0.588	16.56	0.623	15.92	0.483	15.47	<u>0.520</u>	19.31	18.27	17.53
AirNet [40]	18.67	0.752	23.34	0.855	19.03	0.726	-	-	-	-	-	-	-	-	20.34	-	-
PromptIR [82]	22.20	0.825	24.23	0.886	20.86	0.772	-	-	-	-	-	-	-	-	22.43	-	-
MiOIR [90]	<u>24.58</u>	<u>0.892</u>	<u>24.46</u>	0.879	<u>22.42</u>	0.818	<u>19.46</u>	0.661	-	-	<u>18.12</u>	0.561	-	-	<u>23.82</u>	<u>21.80</u>	-
InstructIR [20]	21.57	0.827	23.80	0.838	21.14	0.775	19.21	<u>0.666</u>	-	-	18.06	<u>0.564</u>	-	-	22.17	20.75	-
OneRestore [26]	17.35	0.711	18.70	0.669	16.41	0.617	16.66	0.621	20.24	<u>0.769</u>	-	-	-	-	17.48	-	-
Ours	29.63	0.950	26.93	<u>0.880</u>	26.33	0.875	24.29	0.830	22.71	0.790	21.87	0.735	20.10	0.729	27.63	25.81	24.55
<i>Out-of-distribution</i>																	
MPRNet [97]	15.71	0.636	16.38	0.598	15.57	0.560	14.84	0.345	14.59	0.355	14.58	0.286	<u>14.33</u>	0.299	15.88	15.41	15.14
SwinIR [48]	15.10	0.556	15.79	0.553	14.50	0.486	14.72	0.341	14.32	0.353	14.29	0.282	13.95	0.298	15.13	14.88	14.66
NAFNet [16]	16.77	0.713	19.68	0.751	15.11	0.595	14.40	0.385	14.05	0.390	13.89	0.317	13.27	<u>0.324</u>	17.18	16.00	15.31
Restormer [98]	17.44	0.723	17.31	0.738	17.44	<u>0.723</u>	14.11	0.378	13.59	0.388	13.60	0.314	12.83	0.318	17.39	15.97	15.18
AirNet [40]	17.50	0.732	20.16	0.777	15.07	0.380	-	-	-	-	-	-	-	-	17.57	-	-
PromptIR [82]	19.84	0.797	20.57	0.795	18.22	0.672	-	-	-	-	-	-	-	-	19.54	-	-
MiOIR [90]	<u>20.85</u>	<u>0.850</u>	<u>22.39</u>	<u>0.821</u>	<u>18.87</u>	0.700	15.27	0.406	-	-	<u>14.70</u>	<u>0.332</u>	-	-	<u>20.70</u>	<u>18.41</u>	-
InstructIR [20]	20.33	0.825	19.02	0.636	17.74	0.597	15.34	0.386	-	-	14.52	0.296	-	-	19.03	17.39	-
OneRestore [26]	17.81	0.732	16.77	0.580	15.10	0.595	<u>17.49</u>	<u>0.566</u>	21.04	0.682	-	-	-	-	16.56	-	-
Ours	27.32	0.937	23.82	0.811	23.42	0.801	20.21	0.661	<u>20.15</u>	<u>0.631</u>	17.49	0.529	18.03	0.543	24.85	22.45	21.49

restoration. In addition, we conduct comparisons on both in-distribution (*in-dist.*) and out-of-distribution (*out-dist.*) degradation parameters for mixed-degradation.

We compare our proposed method with task-agnostic methods [16, 48, 97, 98] and all-in-one methods [20, 22, 26, 40, 52, 67, 82, 100]. For fair comparison, we re-train each task-agnostic method with the same experimental settings as ours and employ the publicly released mod-

els of other all-in-one methods. The performance of task-agnostic methods and ours is reported using models trained with 7T (in Tab. 1) and developed mixed degradation space for single-degradation and mixed-degradation, respectively. For other methods, we follow the evaluation setting of [15] and only evaluate on tasks they support. We adopt PSNR and SSIM scores as metrics. In comparison of single-task models, ablation study, and *Suppl.*, we only report PSNR

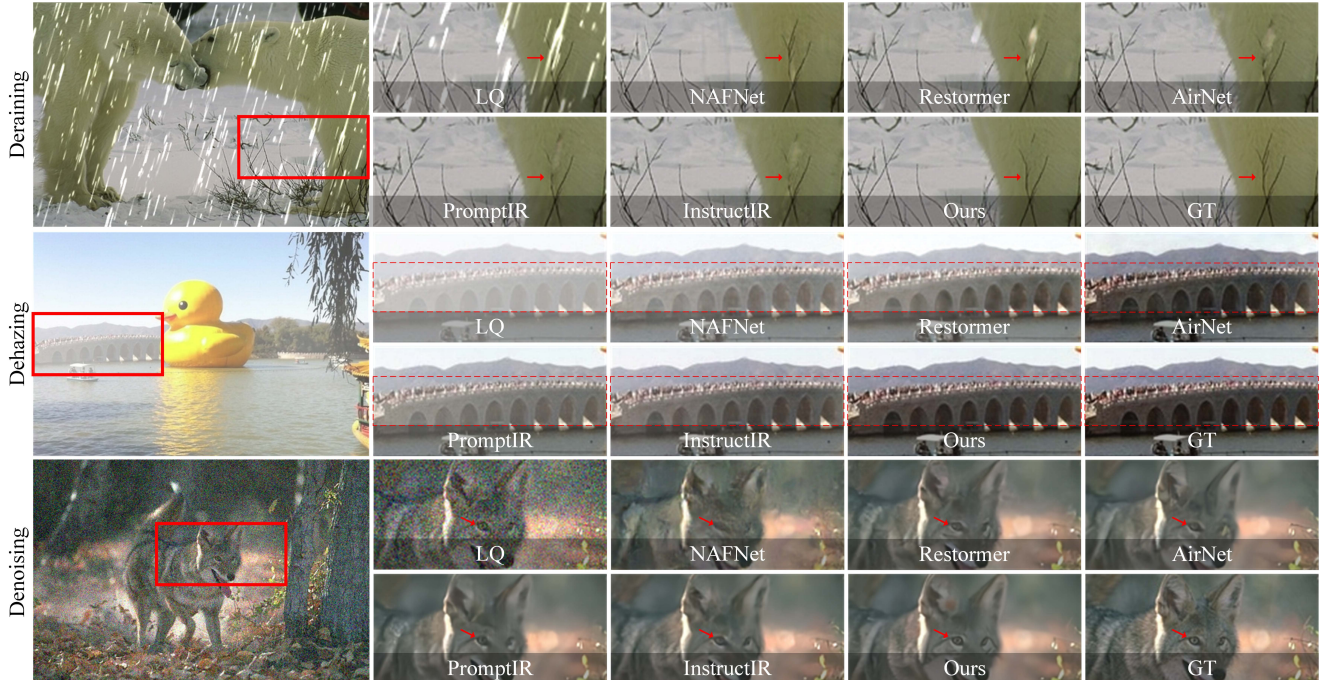


Figure 4. **Visual comparison of results on All-in-One image restoration (single-degradation).** In comparison with others, our method can effectively remove the degradation pattern (*i.e.*, rainstreak, haze, and noise), restore clearer texture (*i.e.*, ‘branches’ and ‘eyes’ pointed by red arrows) and closer color (*i.e.*, bridge in dashed box). More results can be seen in *Suppl.*

Table 3. **Compare to single-task image restoration models.** The task-agnostic methods are trained from scratch on each single-task datasets. Our results are reported without additional single-task training. † denotes *instruction* mode. PSNR scores are reported.

Methods	Derain				Denoise			Desnow			CAR.				Lowlight	Deblur	Dehaze
	200H [95]	200L [95]	DID [99]	DDN [24]	BSD68[61]			Snow100K[57]			LIVE1[76]				LOLv1 [86]	GoPro [64]	SOTS [39]
					$\sigma=15$	$\sigma=25$	$\sigma=50$	S	M	L	$q=10$	$q=20$	$q=30$	$q=40$			
MPRNet [97]	31.53	35.92	35.34	34.19	34.91	32.67	29.62	36.22	34.49	30.63	27.87	30.23	31.57	32.50	23.51	32.66	31.07
SwinIR [48]	29.69	38.35	34.51	33.26	34.81	32.51	29.29	33.45	32.00	28.40	26.16	28.62	29.93	30.81	19.87	29.09	28.35
Restormer [98]	30.98	40.33	35.26	34.16	34.92	32.70	29.70	36.50	34.77	30.86	27.89	30.21	31.56	32.48	23.66	32.92	33.18
NAFNet [16]	29.08	38.93	35.21	32.84	34.80	32.58	29.50	35.94	33.95	29.50	27.95	30.24	31.56	32.47	23.75	33.69	22.70
Ours†	32.01	41.61	35.50	34.40	35.00	32.75	29.75	36.94	35.18	31.14	27.94	30.31	31.66	32.58	27.25	33.71	37.45

scores. Following [67], PSNR and SSIM scores are all calculated in RGB-channels, except that PSNR and SSIM scores are calculated on Y channel of YCbCr color space in comparison of single deraining task [98].

Training Details. For the training of experts, we generally use the AdamW optimizer with batch-size of 8 and patch-size of 128, we take the CosineAnnealing learning rate scheduler with the initial learning rate of $3e^{-4}$. After the training, the weights of experts are frozen, and we train degradation and granularity estimation based routers. For the training of routers, we adopt Adam optimizer with batch-size of 8 and patch-size of 256, we adopt a fixed learning rate of $1e^{-3}$, and we set α to 0.1 and β to 0.01 in Eq. (9). All experiments are trained on 8 NVIDIA A6000 GPUs. More details of the experimental setups and training details can be seen in *Suppl.*

4.2. Comparison with State-of-The-Art Methods

Comparison with All-in-One Models. With the increasing number of restoration tasks, it is difficult for the tailored all-in-one methods to have obvious performance gain over SOTA task-agnostic methods. Our method can significantly outperform task-agnostic and all-in-one methods by a large margin in single-degradation setup (Tab. 1 and Fig. 4). In mixed-degradation, our method continuously achieves higher performance than task-agnostic and all-in-one methods from simple to complex mixed degradation (Tab. 2). In addition, comparisons on *out-dist.*, *real-world* (Tab. 8), and *unseen* (see Tab. F in *Suppl.*) image restoration datasets reveal that our method also guarantees better generalization performance than others. More visual comparison results can be seen in *Suppl.*

Comparison with Single-Task Models. For a fair comparison, we evaluate the performance of our method in *instruc-*

Table 4. Effect of DR extractors.

Methods	Rain	Rain	Test	Test
	200H	200L	1200	2800
VGG [78]	31.47	40.59	35.26	34.18
DDR [54]	30.97	40.37	35.25	34.17
DA-CLIP [59]	31.65	40.67	35.24	34.12
Manual div.	31.88	41.43	35.32	34.23
Ours	32.01	41.61	35.50	34.40

Table 5. Effect of fineness.

# DRs	MiO (Average)	
	<i>In-dist.</i>	<i>Out-dist.</i>
1	22.06	17.23
2	22.42	17.51
4	23.75	18.49
8	24.22	18.35
16	24.30	18.44

Table 6. Effect of #granularities.

# Levels	{ # DRs }	MiO (Average)	
		<i>In-dist.</i>	<i>Out-dist.</i>
1	{ 8 }	24.22	18.35
2	{ 1, 8 }	24.27	18.86
2	{ 4, 8 }	24.44	19.06
3	{ 1, 4, 8 }	24.46	19.45
4	{ 1, 4, 8, 16 }	24.41	19.47

Table 7. Effect of the routers

Method	\mathcal{G}_d	\mathcal{G}_g	MiO (Average)	
			<i>In-dist.</i>	<i>Out-dist.</i>
Clustering			17.01	14.19
Only \mathcal{G}_d	✓		24.34	18.60
Ours	✓	✓	24.46	19.45

Table 8. Generalization performance on real-world datasets. All methods are evaluated without training on corresponding training data.

Methods	Deraining		Low-light Enh.		Desnowing		Average	
	LHP [25]		LOLv2-real [92]		RealSnow [115]			
	PSNR	SSIM	PSNR	SSIM	PSNR	SSIM	PSNR	SSIM
MPRNet [97]	29.16	0.884	9.67	0.170	25.82	0.831	27.10	0.821
SwinIR [48]	21.74	0.803	18.67	0.730	18.45	0.723	20.91	0.783
NAFNet [16]	26.04	0.838	26.46	0.861	<u>27.51</u>	<u>0.881</u>	26.33	0.847
Restormer [98]	27.23	0.862	28.92	0.898	26.73	0.875	27.26	0.866
PromptIR [67]	25.68	0.856	-	-	-	-	-	-
MiOIR [90]	28.69	0.877	10.62	0.284	-	-	-	-
InstructIR [20]	28.93	0.893	<u>30.31</u>	0.909	-	-	-	-
OneRestore [26]	24.55	0.796	17.76	0.657	20.12	0.726	23.24	0.773
Ours	30.04	<u>0.886</u>	30.40	<u>0.901</u>	28.04	0.888	29.70	0.887

tion mode (Ours[†]). As shown in Fig. 3, each task instruction corresponds to a binary mask. Based on the mask, we prune out the unrelated expert models, leaving the corresponding experts as a sub-model of the original trained multi-granularity MoE model. We then allocate experts based on degradation and granularity estimation for given corrupted inputs. As shown in Tab. 3, by learning image degradation in finer granularity, and utilizing pruning to alleviate degradation estimation error, our method can outperform single-task models without additional training.

4.3. Ablation Study

Effect of DR Extractors. In Tab. 4, we learn experts using data clustered by different DR extractors, including VGG [78], DDR [54], DA-CLIP [59], manually division by publicly released dataset (Manual div.), and our method. Our learned \mathcal{D} can distinguish finer-grained DR, we thus can learn deraining task in finer-grained level, allowing our experts achieve better performance than others.

Effect of DR Fineness. In Tab. 5, we group the degradation space into different numbers of DR groups (from 1 to 16), with grouped into finer-grained DR groups, the performance on *in-dist.* steadily improves. However, with increasing difficulty of routing, performance does not have a marginal improvement when #DRs more than 8. For generalization performance, clustering DR groups in proper coarse-grained level performs better than finer-grained levels, indicating that it is essential to combine multiple granularities to keep performance on both *in-dist.* and *out-dist.*

Effect of Multiple Granularities. We evaluate the performance of different combinations of granularity. As shown in Tab. 6, with granularity estimation, incorporat-

ing both fine-grained levels and coarse-grained levels can maintain much better restoration performance and generalization ability than employing single granularity. Taking performance, training cost, and learning difficulty into account, we finally adopt $\{1, 4, 8\}$ in our experiments.

Effect of \mathcal{G}_d and \mathcal{G}_g . Using both \mathcal{G}_d and \mathcal{G}_g can benefit more accurate routing. \mathcal{L}_{load} can avoid routing to collapse to the finest-grained level, improving performance on *out-dist.* Without using any routers, clustering method confused DRs in different granularities and the cannot guarantee the right routing results, leading to lower performance.

Others. We provide more experiments and discussion in the *Suppl.* First, we statistic the computational cost (e.g., #FLOPs, latency, #parameters, GPU memory consumption, and training time) in Tab. A and Tab. B. Second, to align the inference cost with some compared methods, we use smaller experts to conduct experiments in Tab. B. Third, to align the training #parameters of some compared methods with ours, we scale up Restormer [98] and PromptIR [67] models (named Restormer-L and PromptIR-L, respectively) to conduct experiments in Tab. C. Fourth, we further analyze the proposed routing method in Sec. H, including routing accuracy (see Tab. D) and the impact of loss functions (see Tab. E). Fifth, we discuss the reasons of deploying full-model as expert in Sec. F.

5. Conclusion

In this paper, we introduced our UniRestorer, a new universal image restoration framework that aims to leverage degradation priors to improve restoration performance while alleviating the inevitable error in degradation estimation. We learn all-in-one image restoration in multiple granularities and propose to estimate image degradation at proper granularity. Specifically, we perform hierarchical clustering on degradation space and develop a multi-granularity degradation set as well as a MoE restoration model. Besides vanilla degradation estimation, granularity estimation is further introduced to indicate the degree of degradation estimation error. By adopting both degradation and granularity estimation, we train routers to adaptively allocate unknown corrupted inputs to the most appropriate expert. Experimental results demonstrate our superior performance and promising potential in closing the performance gap to specific single-task models.

UniRestorer: Universal Image Restoration via Adaptively Estimating Image Degradation at Proper Granularity

Supplementary Material

The content of the supplementary material involves:

- Dataset usage in Sec. **A**.
- Degradation pipeline and parameters in Sec. **B**.
- Training details in Sec. **C**.
- Implementation details in Sec. **D**.
- Overhead comparison in Sec. **E**.
- MoE design choice in Sec. **F**.
- Comparison with vanilla scaling up in Sec. **G**.
- Routing analysis in Sec. **H**.
- Limitation and future works in Sec. **I**.
- More results and visual comparisons in Sec. **J**.

A. Dataset

In this section, we detail the usage of datasets in training our models on single-degradation and mixed-degradation: **(1)** Single-degradation: For training, we adopt Rain100L [95] dataset for deraining, RESIDE [39] dataset for dehazing, DFBW (DIV2K [2], Flickr2K [50], BSD [61], and WED [60]) datasets for Gaussian color image denoising and compression artifacts removal, GoPro [64] dataset for motion deblurring, LOLv1 [86] dataset for low-light enhancement, Snow100K [57] dataset for desnowing. Following [67, 100], We evaluate our method on Rain100L [95] for deraining, SOTS [39] for dehazing, BSD68 [61] for Gaussian color image denoising, GoPro [64] for motion deblurring, LOLv1 [86] for low-light enhancement, Snow100K-L [57] for desnowing, and LIVE1 [76] for compression artifacts removal. **(2)** Mixed-degradation: In mixed-degradation, we synthesize mixed degradation datasets from clean images in DF2K (DIV2K [2] and Flickr2K [50]) datasets for training and evaluation, respectively. The degradation pipeline can see Fig. **A**. **(3)** Single-task comparison: Rain100L dataset is limited by its scale. To enlarge degradation space and the number of training data for deraining task, we collect Rain200H [95], Rain200L [95], DID [99], and DDN [24] as training data. Based on the clustered results, we retrain experts for degradation set related to rain degradation and replace original deraining experts used in single-degradation into newly trained ones. For other tasks, we keep the same with datasets used in single-degradation. **(4)** Ablation study: Since the effectiveness of our method can be revealed in both performance

on in-distribution and out-of-distribution samples, we conduct ablation study on mixed-degradation. To simplify the evaluation process, we adopt Urban100 [65] as high-quality clean data and the same degradation pipeline as **(2)**.

B. Degradation Pipeline and Parameters

Degradation Pipeline. We follow the degradation pipeline of [106] to construct synthetic low-quality datasets for the training of the degradation extractor and all-in-one image restoration in mixed-degradation setup. As shown in Fig. **A**, given high-quality clean inputs y , we orderly add synthetic lowlight, blur, noise, rain, snow, and haze to synthesize corresponding low-quality outputs x . We adopt gates between different degradations to gap one of them probably, the probability of all gates is generally set to 0.5. The way of each degradation is introduced as follows:

Blur. Following [102], we synthesize blurring degradation as,

$$x = y \otimes k, \quad (\text{A})$$

where k is the blur kernel. In our implementation, the type of blur kernel includes isotropic and anisotropic, each of which is employed with the probability of 0.5. The kernel size is sampled in the range from 7 to 23. The standard deviation of the Gaussian kernel is set from 1 to 3 for *in-dist.* and 3 to 4 for *out-dist.*

Noise. Gaussian noise is synthesized as,

$$x = y + n, \quad (\text{B})$$

where n is Gaussian noise with variance σ^2 . σ is set from 15 to 35 for *in-dist.* and 35 to 50 for *out-dist.*

Rain. Raining degradation is synthesized as,

$$x = y + r, \quad (\text{C})$$

where r is rain streaks. Following [90], r is synthesized with random noise and Gaussian blur, where noise is related to the strength of the rain, and blur kernel is related to the rain direction, length, and width. We adopt the number of rain streaks from 50 to 100 in *in-dist.* and 100 to 150 for *out-dist.* Rain direction is generally adopted from -45° to 45° , rain length is set from 20 to 40, and rain width is uniformly sampled from $\{3, 5, 7, 9, 11\}$.

Haze. Following [39], hazing degradation is synthesized as,

$$x = T(y)y + a(1 - T(y)), \quad (\text{D})$$
$$T(y) = e^{-\beta D(y)},$$

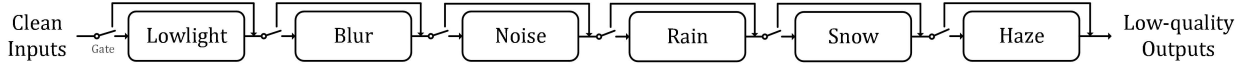


Figure A. Degradation Pipeline.

where a is the global atmospheric light, $T(y)$ is the transition matrix, $D(y)$ is the depth map, and β is the scattering coefficient of the atmosphere. In haze degradation synthesizing, the value of β largely decides the thickness of haze. We adopt one publicly released project MegaDepth¹ to estimate the depth image. In our experiments, the global atmospheric light is set from 0.8 to 1, the β is set from 0.5 to 1.5 for *in-dist.* and 1.5 to 2 for *out-dist.*

Snow. Snowing degradation is synthesized as,

$$x = y \times (1 - m) + m, \quad (\text{E})$$

where m is the snow mask randomly sampled from Snow100K [57] dataset.

Lowlight. Following [26], lowlight degradation is synthesized as,

$$x = \frac{y}{I(y)} I(y)^\gamma \quad (\text{F})$$

where $I(y)$ is the illusion map obtained from RetinexFormer [11] and γ is the darkening coefficient. Since we explicitly include noise degradation in our degradation pipeline, we do not additionally consider noise in this step. We set γ from 1 to 2 for *in-dist.* and 2 to 2.5 for *out-dist.*

Besides, JPEG compression is synthesized by employing the publicly released project DiffJPEG².

C. Training Details

Training of DR Extractor. To train our degradation representation (DR) extractor, we adopt the above ways to synthesize various types of low-quality data. According to the parameter that decides the degradation degree, we separate synthetic data into multiple groups. For deraining degradation, strength from 0 to 50 is small rain, 50 to 100 is medium rain, and 100 to 150 is large rain; In denoising, σ of Gaussian noise from 0 to 15 is small noise, 15 to 35 is medium noise, and 35 to 50 is large noise; In dehazing, scattering coefficient β larger than 0.1 is thick haze, β smaller than 0.1 is normal haze; In deblurring, kernel size of motion blur kernel larger than 15 is large blur, kernel size smaller than 15 is small blur; In desnowing, we use snow masks from Snow100K dataset and adopt the official separation. In compression artifacts removal, image quality from 0 to 15 is large compression, 15 to 35 is medium compression, 35 to 50 is small compression; In lowlight enhancement, the darkening coefficient from 1 to 1.5 is light corruption and 1.5 to 3 is heavy corruption.

¹<https://github.com/zhengqili/MegaDepth>

²<https://github.com/mlomnitz/DiffJPEG>

Training of Experts. In the training of experts, we first conduct hierarchical clustering based on collected datasets, after that, all degraded training images are divided into multiple groups in different granularities. In each granularity, we record for each group the data samples that is allocated to it. Then, we use the recorded data to train expert restoration network for each group.

Training of Routers. After training of experts, the weights of experts are frozen, and we train degradation and granularity estimation based routers. Most works in high-level vision and NLP tasks train experts and routers jointly, to well deal with the conflicts between restoring different degradations, MoE system in image restoration works or all-in-one image restoration works prefer separate training [4, 13, 15, 66, 81, 115], *i.e.*, sequentially training experts and routers. Similarly to the mentioned works, our experts are explicitly determined to solve degradations in each degradation set, experts should be learned in advance and are not affected by the routers to guarantee the stability of the whole model. Thus, we learn experts and routers sequentially rather than simultaneously.

D. Implementation Details

Multi-Granularity MoE Restoration Model. To construct our MoE restoration model, we adopt Restormer [98] as the expert model for most of the tasks, except for lowlight enhancement, for which we choose RetinexFormer [11] as the expert model. In single-degradation setting, we set two experts for lowlight enhancement, deblurring, and dehazing to learn to restore light corruptions and heavy corruptions, respectively. We set three experts for desnowing, denoising, and CAR to learn light corruptions, medium corruptions, and heavy corruptions, respectively. Considering the diversity of rain degradation, we adopt four experts for deraining task. As a result, our MoE restoration model has three granularities. In the coarsest-grained level, we use one expert model to solve all observed degradations; in the second level, we use seven experts to solve different tasks; and in the finest-grained level, we totally have nineteen experts, and each expert is responsible for one specific type of degradation with specific degradation degree.

Structure of \mathcal{H} and \mathcal{G} . Without dedicated design, we adopt 5-layer MLP for both \mathcal{H}_d and \mathcal{H}_g , in which the number of input and output channels is 512 (the same with the dimension of DR e). The structure of \mathcal{G}_d and \mathcal{G}_g is one-layer MLP with input channels of 512 and the number of output channels equal to the number of experts.

Ours[†]. The *instruction* mode of our method allows infer-

Table A. Overhead comparisons.

Methods	#FLOPs (G)	Latency (s)
Restormer [98]	1128.9	0.368
NAFNet [16]	505.5	0.186
PromptIR [67]	1266.2	0.355
OneRestore [26]	94.5	0.238
Ours	1155.8	0.484

Table B. All-in-One image restoration results (three tasks single-degradation). We replace original experts with smaller NAFNet (NAF.) and Restormer (Res.) as experts. ‘Inf.’ means during inference. The reported Params. mainly includes restoration networks.

Methods	Derain	Dehaze	Denoise	#FLOPs (G)	Latency (s)	Params.(M) Inf./Train	Mem. (M) Inf.	Time(h) Train
	Rain100L	SOTS	BSD68					
PromptIR [67]	36.37	30.58	31.12	1266.2	0.355	39.6/39.6	3552	201
Ours	41.68	36.44	31.43	1155.8	0.484	26.1/339.3	4258	578
Ours (NAF.)	38.98	31.69	31.28	154.7	0.156	17.1/222.4	1818	169
Ours (Res.)	41.41	35.38	31.35	672.7	0.395	14.8/192.5	3526	442

Table C. All-in-One image restoration result (mixed-degradation). ‘Inf.’ means during inference. ‘-L’ indicate large scale version of model. The reported Params. mainly includes restoration networks. PromptIR-L is trained in FP16.

Methods	MiO (Avg.)	#FLOPs (G)	Latency (s)	Params.(M) Inf./Train	Mem. (M) Inf.	Time (h) Train
	In/out-dist.					
Restormer	22.06 /17.23	1128.9	0.368	26.1/26.1	3244	48
Restormer-L	23.98 /18.65	17360.1	1.375	441.8/441.8	13408	3792
PromptIR-L	24.13 /18.76	18139.6	1.283	439.3/439.3	12962	-
Ours	24.46/19.45	1155.8	0.484	26.1/339.3	4258	578

ence based on given task instructions, *i.e.* the task name. In our implementation, the task instructions can convert to specific binary masks, which represent pruning or not pruning on the corresponding expert model in our MoE restoration model. According to the masks, we first prune out the corresponding expert models, then we conduct degradation- and granularity-based routing to find the most appropriate expert model for corrupted inputs. In this way, the error in degradation estimation is alleviated, the routing accuracy is highly improved, and thus the restoration performance is further improved.

Ablation Study on DR Extractors. We adopt pre-trained vgg16, pre-trained ESRGAN on bicubic $4\times$ super-resolution, and pre-trained DACLIP as DR extractors, and evaluate their effect on expert restoration model. We conduct experiments on the deraining task. We first extract DRs for all low-quality inputs, we cluster the obtained representation into four clusters, and for each cluster of samples we train one expert. Since we exploit DR at a finer-grained level, the experts we trained can achieve better performance than others.

E. Overhead Comparisons

We calculate FLOPs and latency with $512 \times 512 \times 3$ input, on a single NVIDIA A6000 GPU. As shown in Tab. A, thanks to mixture-of-experts, the overhead of our method is

slightly higher than Restormer [98]. As a result, our method can achieve high restoration accuracy and low latency simultaneously.

F. MoE Design Choice

Using Full-Network or Sub-Network as Expert. MoE is an effective solution to training large models in high-level vision and NLP tasks. A way is to deploy sub-networks as experts based on one shared backbone weight. For example, in all-in-one image restoration, some works [66, 115] adopt such a way to develop their MoE system for alleviating conflict among different restoration tasks. Another way is to use a full-network as an expert directly. For examples, early work [87] in real-world super-resolution has adopted this way. Recent all-in-one image restoration works [13, 15] also develop the restoration expert using the full-network. In our work, using full-network and sub-network as an expert have similar computational cost. However, using full-network can have some advantages. First, it is easier to build and expand. Second, it can assign its full parameters for specific degradation, which has a more powerful fitting ability. Third, we can benefit much from the previous advanced architecture design towards specific tasks, unleashing their full power in solving all-in-one image restoration topic.

More Lightweight Experts. We have designed more lightweight experts (by scaling down Restormer [98] and NAFNet [16]) and provided complexity analysis in Tab. B. It shows that it achieves obvious performance gains with a much smaller inference cost than PromptIR [67].

G. Compare to Vanilla Scaling Up

According to its degradation estimation and the estimation error, the routers select the most appropriate expert for each input low-quality image, leading to a sparse inference strategy (see Tab. B and Tab. A). Though our method has comparable inference parameters, FLOPs, and latency with methods in similar backbone, one may know the effect of training parameters. To mitigate the gap of training parameters, we scale up the model size of Restormer and PromptIR to be similar as ours in training parameters, and we conduct experiments on mixed-degradation. As shown in Tab. C, after scaling up training parameters, Restormer-L and PromptIR-L cannot have marginal performance gains, it reveals that simply increasing the model size is not the essence of improving the performance, which is different from the scaling law in high-level vision and NLP tasks. In this view, our method provides an effective way to scaling up low-level vision image restoration model meanwhile can effectively improve its performance.

Table D. Routing accuracy.

Level	<i>in-dist.</i>	<i>out-dist.</i>
	0 / 1 / 2	0 / 1 / 2
Expected	7 / 13 / 80	29 / 46 / 25
Practical	5 / 17 / 78	34 / 50 / 16

Table E. Effect of loss functions.

ℓ_1	\mathcal{L}_{dg}	\mathcal{L}_{load}	MiO (Average)	
			<i>In-dist.</i>	<i>Out-dist.</i>
✓			24.14	18.37
✓	✓		24.35	18.76
✓	✓	✓	24.46	19.45

Table F. Generalization performance on unseen degradations. All methods are evaluated without training on corresponding training data. PSNR scores are reported.

Methods	Raindrop Remvoal	UDC-IR	Underwater-IR
	Raindrop [69]	TOLED [113]	UIEB [41]
NAFNet [16]	22.89	26.89	15.54
Restormer [98]	23.34	28.44	15.80
PromptIR [67]	22.98	25.02	16.12
MiOIR [90]	23.59	20.11	16.26
OneRestore [26]	22.02	15.16	15.87
Ours	24.91	29.64	18.07

H. Routing Analysis

Routing Accuracy If degradation estimation (DE) on the finest granularity level is accurate, using experts on leaves is preferred. However, fine-grained DE is error-prone. The proposed granularity estimation measures the uncertainty of DE. When the uncertainty is large, it means that the finest-grained expert is probably not suitable for this degradation. Instead, a coarser-grained expert is more robust to estimation error, thus being selected. The results in Tab. 6 indicate using multiple granularity combination is better on both *in-dist.* and *out-dist.* In Tab. D, we also report the practical #loads and expected #loads (by maximizing PSNR) of different granularity levels during inference on Urban100 dataset with mixed-degradation, and our routing accuracies are respectively 92% and 82% on *in-dist.* and *out-dist.*

Effect of Loss Functions As shown in Tab. E, both \mathcal{L}_{dg} and \mathcal{L}_{load} can benefit more accurate routing. In particular, \mathcal{L}_{dg} and \mathcal{L}_{load} can avoid the routing to collapse to the finest-grained level, improving performance on *out-dist.*

I. Limitation and Future Works

On the one hand, the training data mainly comes from publicly released datasets, with requirement of comparing to baseline methods. However, the scale of training data is essential, particularly in developing large-scale models. In image restoration works, the training data is generally small, *e.g.* Rain100L [95] only has 200 pairs of training data. Previous works [85] had exploited the benefits brought by scaling up the training data, we thus plan to collect more high-quality training data to bring further improvement on our method. On the other hand, we plan to expand and align our degradation space with real-world scenarios, aiming to well restore real-world image degradations.

J. More Results and Visual Comparisons

Results on Unseen Degradations. As shown in Tab. F, without additional training on specific data, our method can outperform other task-agnostic methods and all-in-one methods on restoring unseen degradations, *e.g.*, raindrop removal, under-display camera image restoration, and underwater image restoration, demonstrating the generalization ability of our method.

More Visual Comparisons. We show more visual comparison results in this section. Compared to task-agnostic methods, all-in-one methods, and specific single-task models, our method can restore more clear results with detailed textures. The single-degradation results of all-in-one image restoration comparisons can be seen in Fig. B to Fig. H. The comparison results with specific single-task models can be seen in Fig. I to Fig. N. In the evaluation of mixed degradation, since the resolution of images from DIV2K-valid is too high, limiting inference on the whole image for all methods. We first crop high-resolution images into overlapped 512×512 crops, after inference, we inverse the cropping process and recombine crops back to one whole image, though averaging the overlapped area, the border artifacts cannot be avoidable. Comparison result of *in-dist.* and *out-dist.* can be seen in Fig. O and Fig. P, respectively.

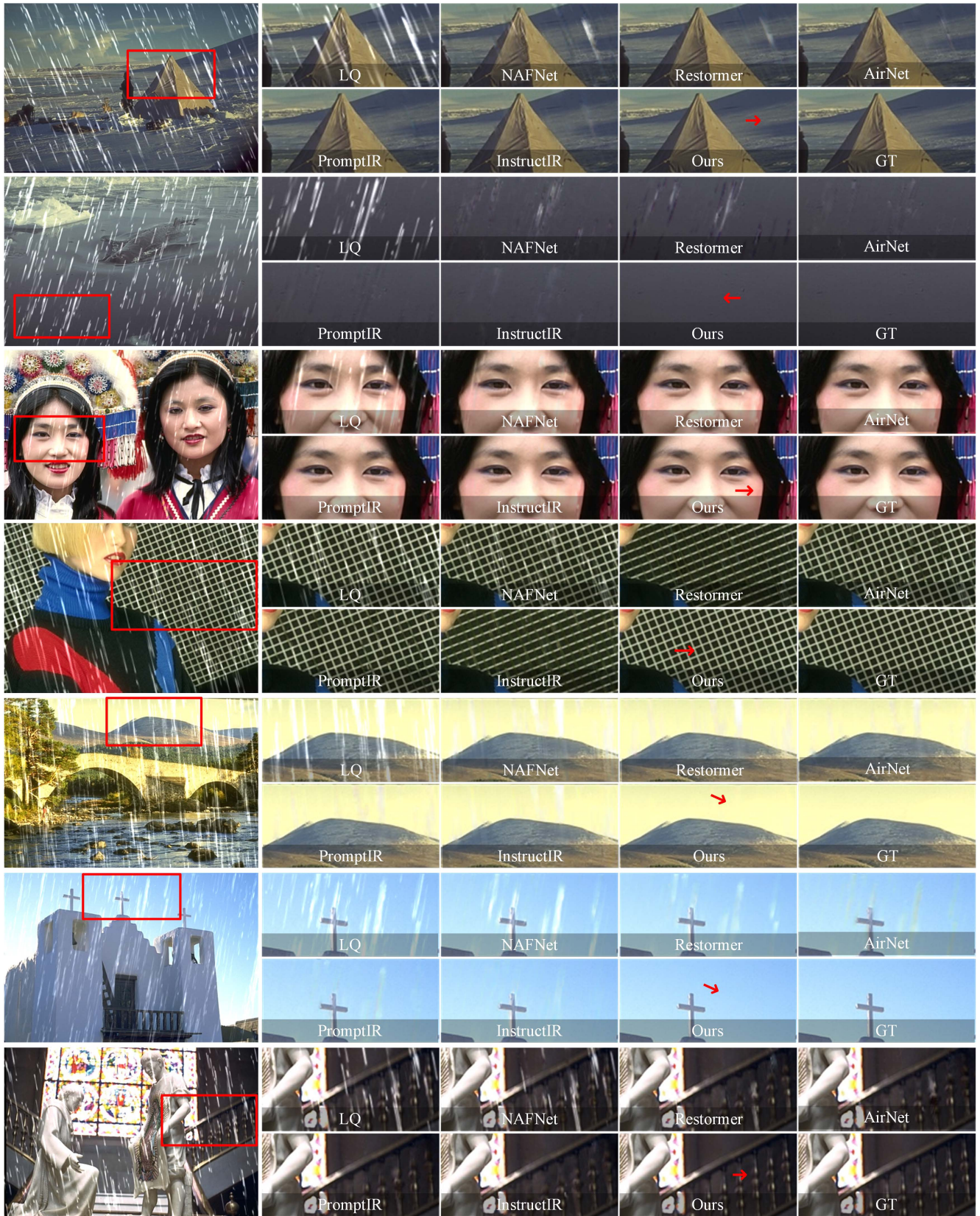


Figure B. Visual comparison of results on All-in-One image restoration (deraining).

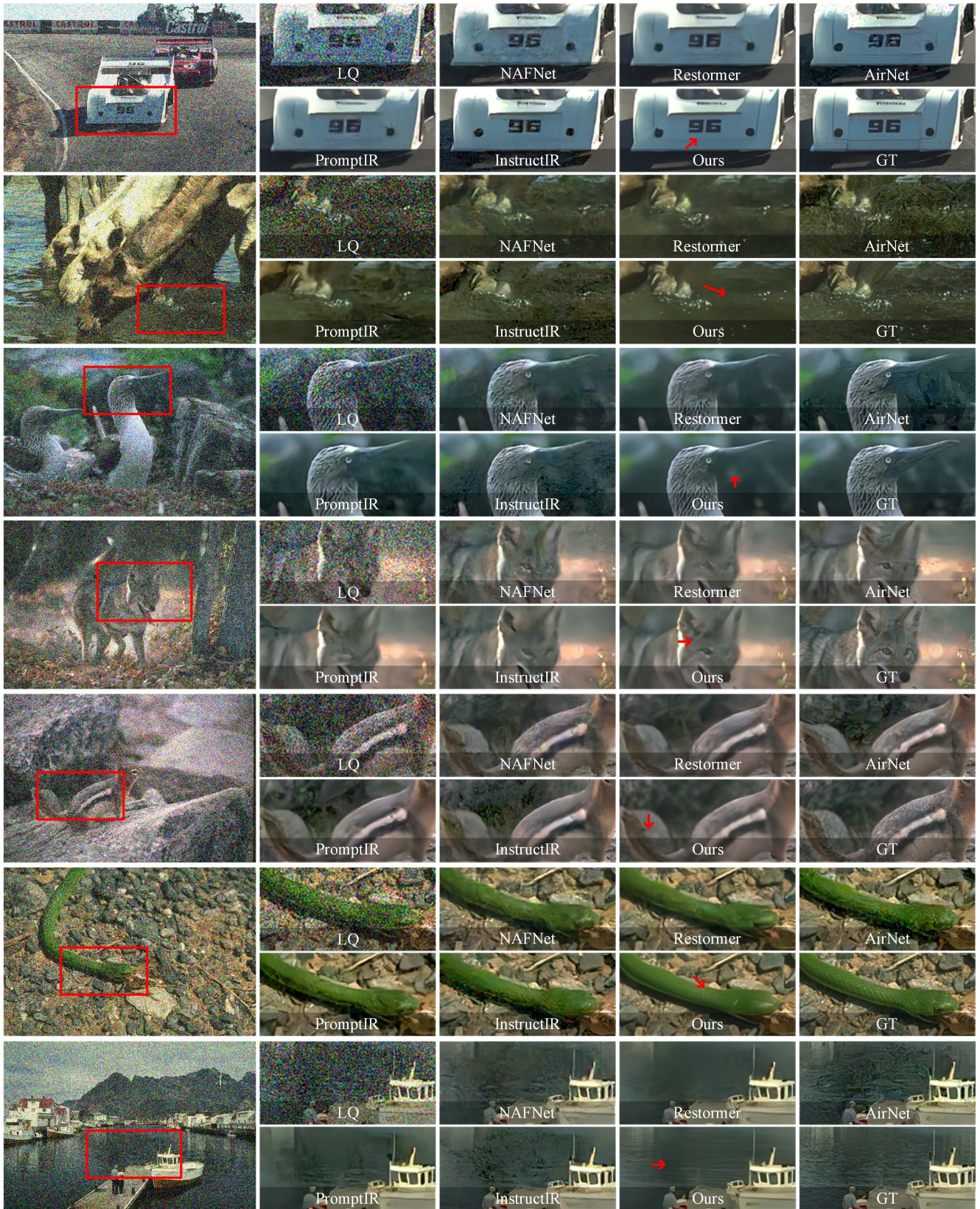


Figure C. Visual comparison of results on All-in-One image restoration (Gaussian-denoising).



Figure D. Visual comparison of results on All-in-One image restoration (dehazing).

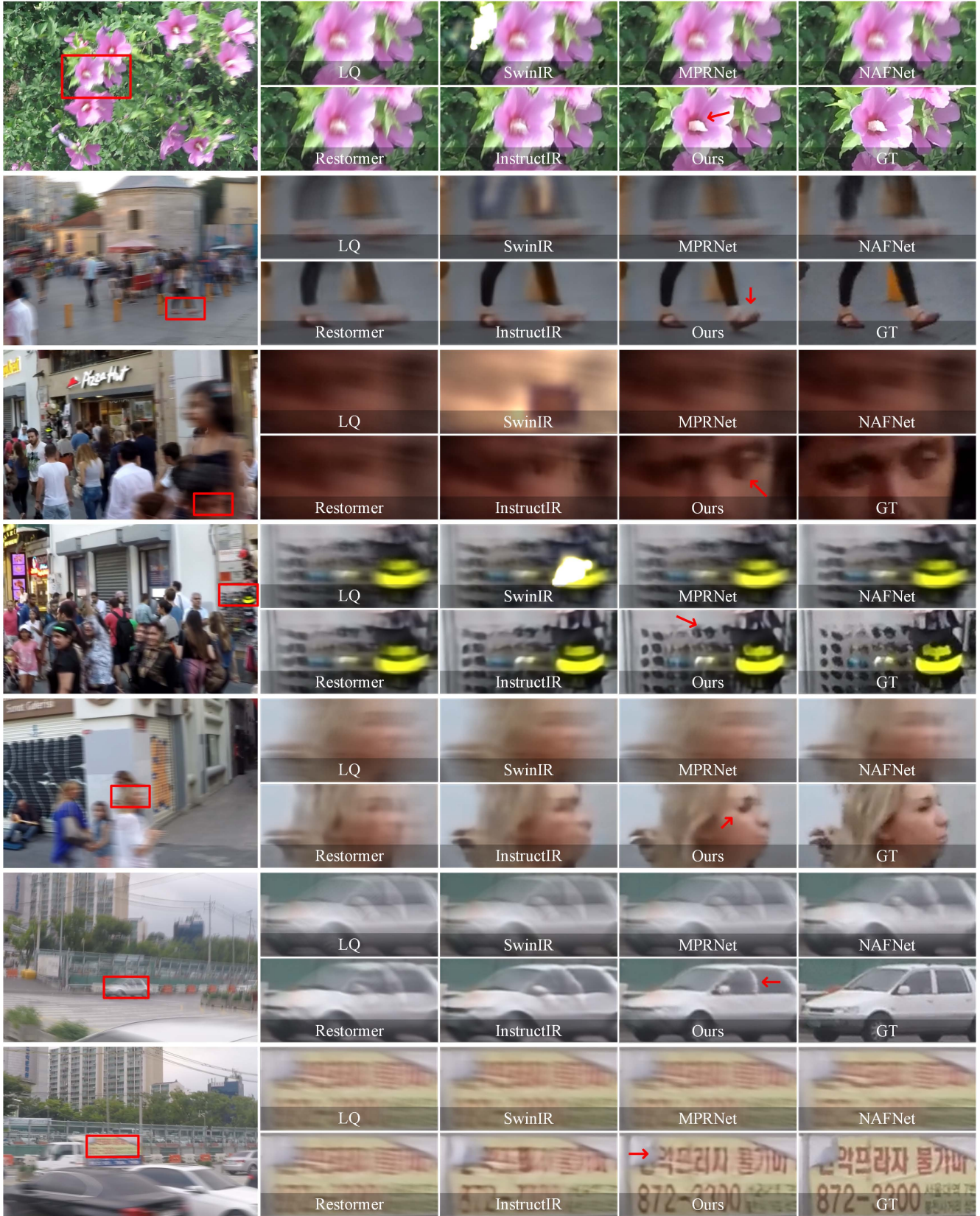


Figure E. Visual comparison of results on All-in-One image restoration (motion-deblurring).

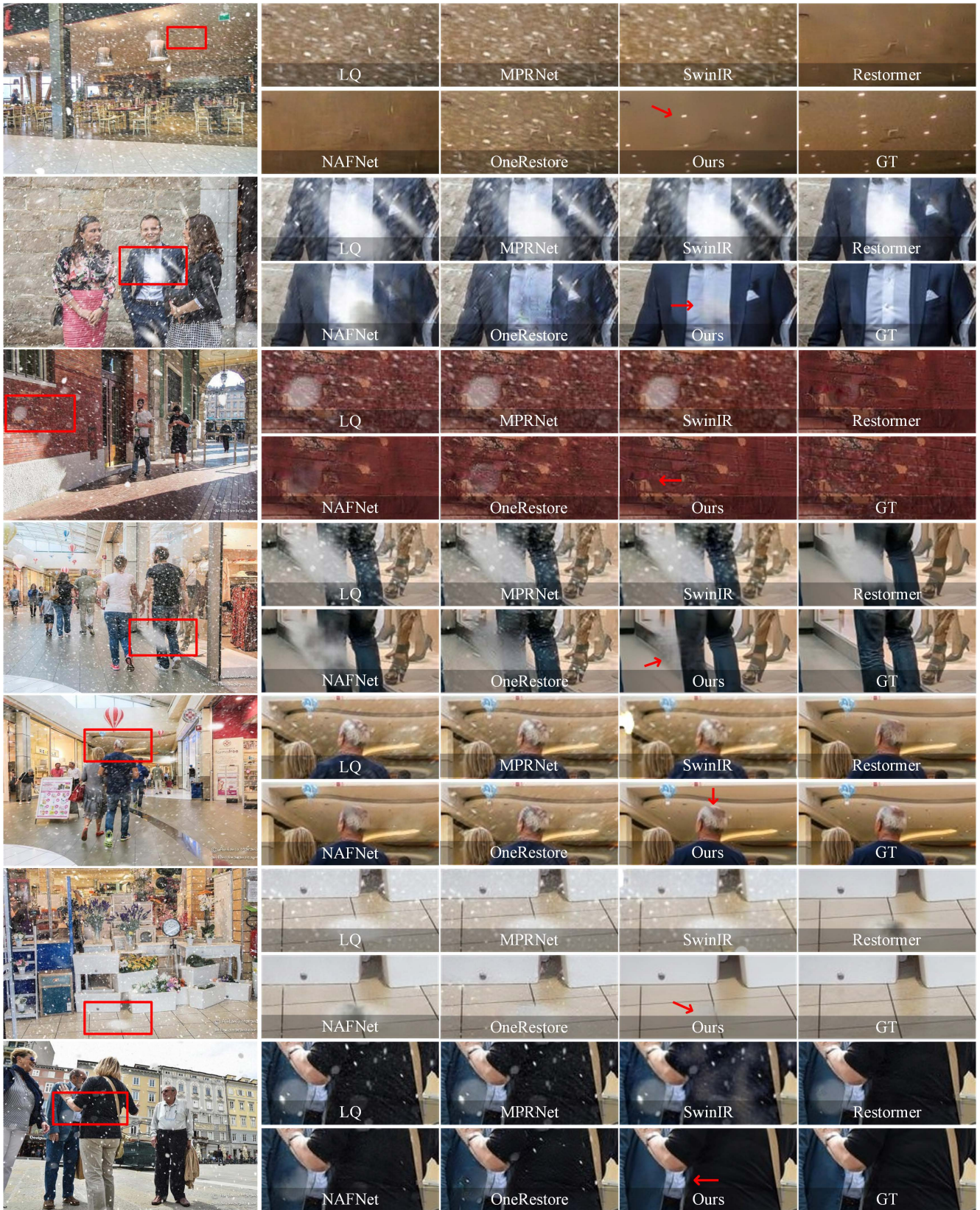


Figure F. Visual comparison of results on All-in-One image restoration (desnowing).

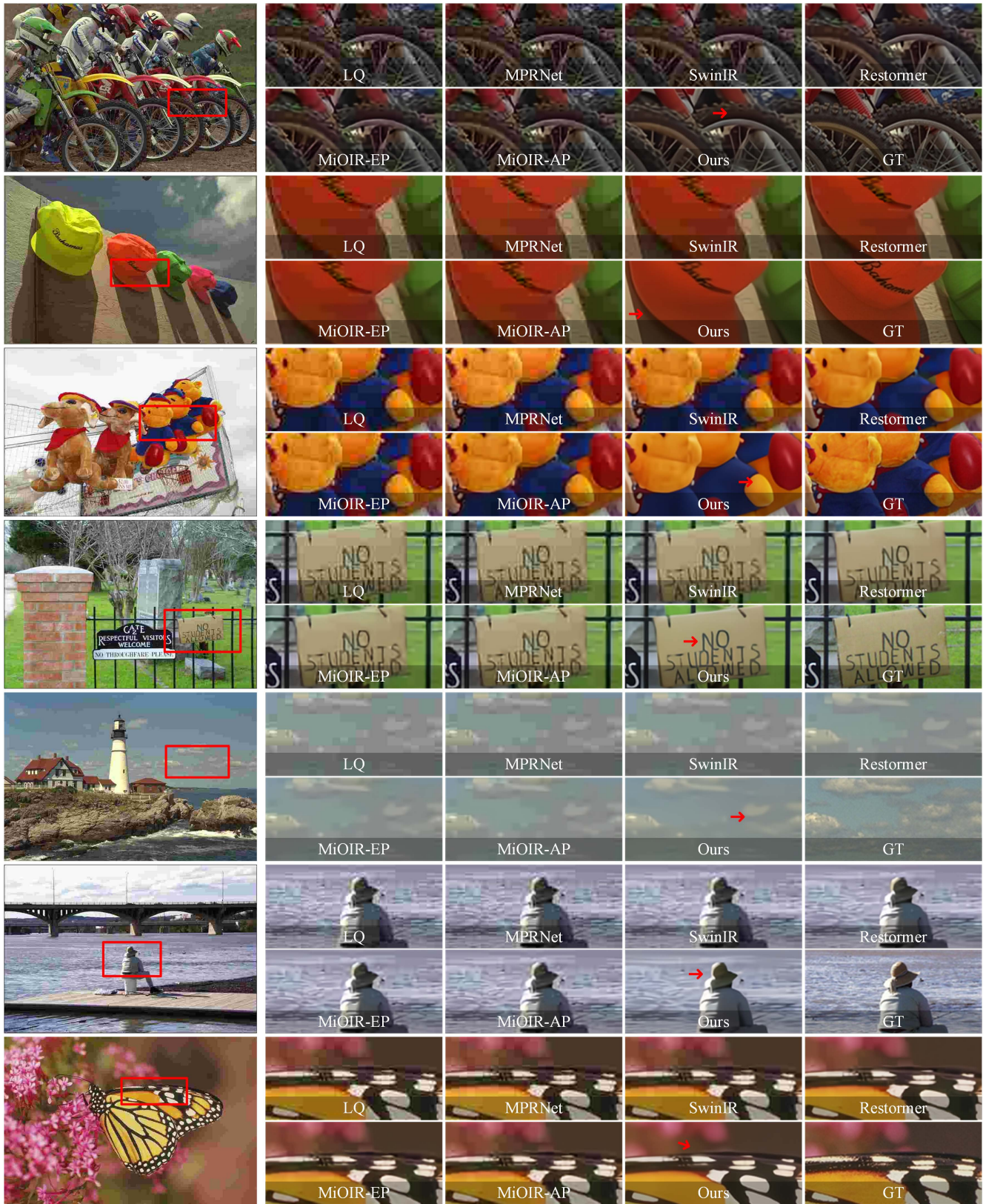


Figure G. Visual comparison of results on All-in-One image restoration (compression artifacts removal).

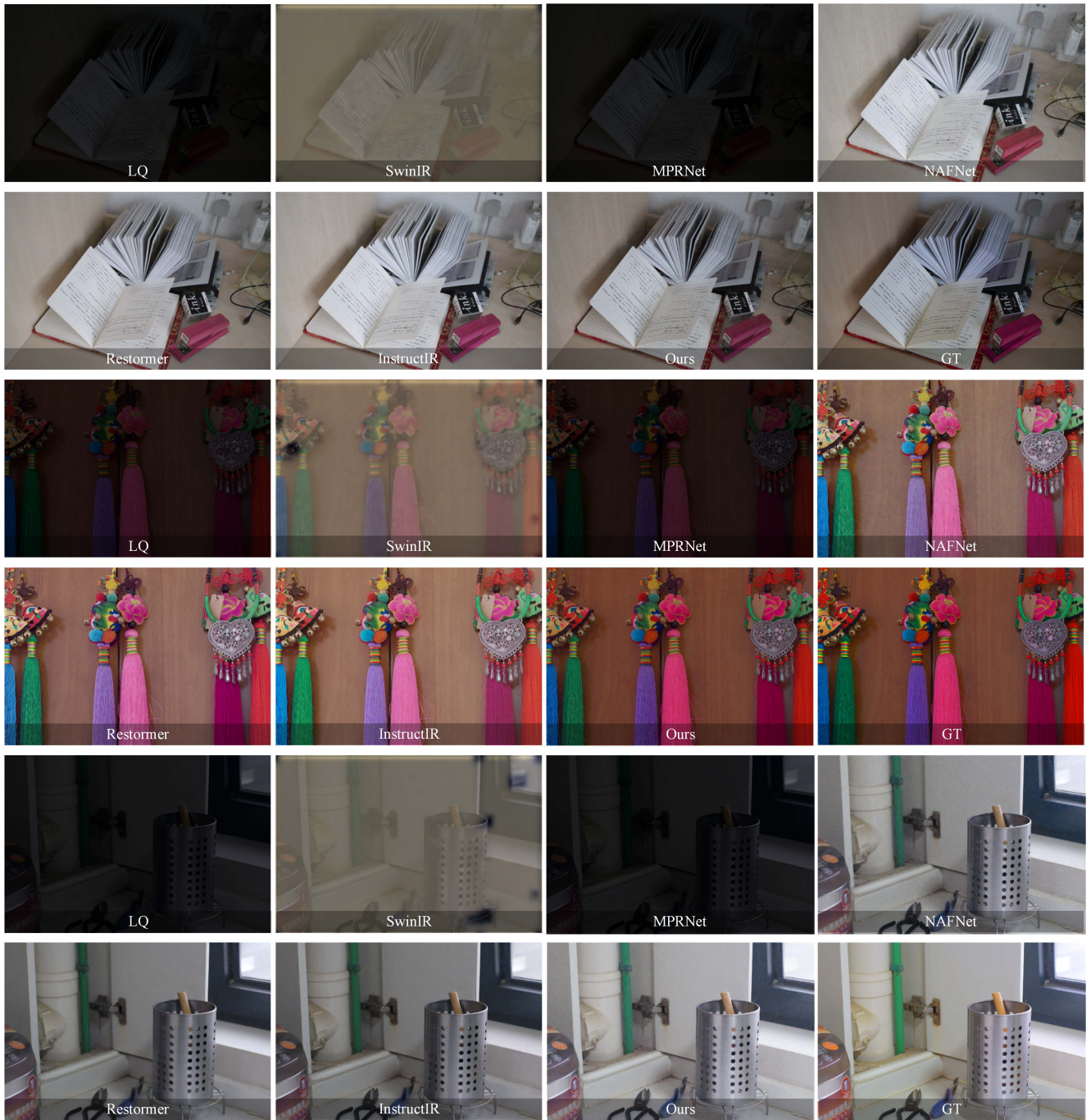


Figure H. Visual comparison of results on All-in-One image restoration (lowlight enhancement).

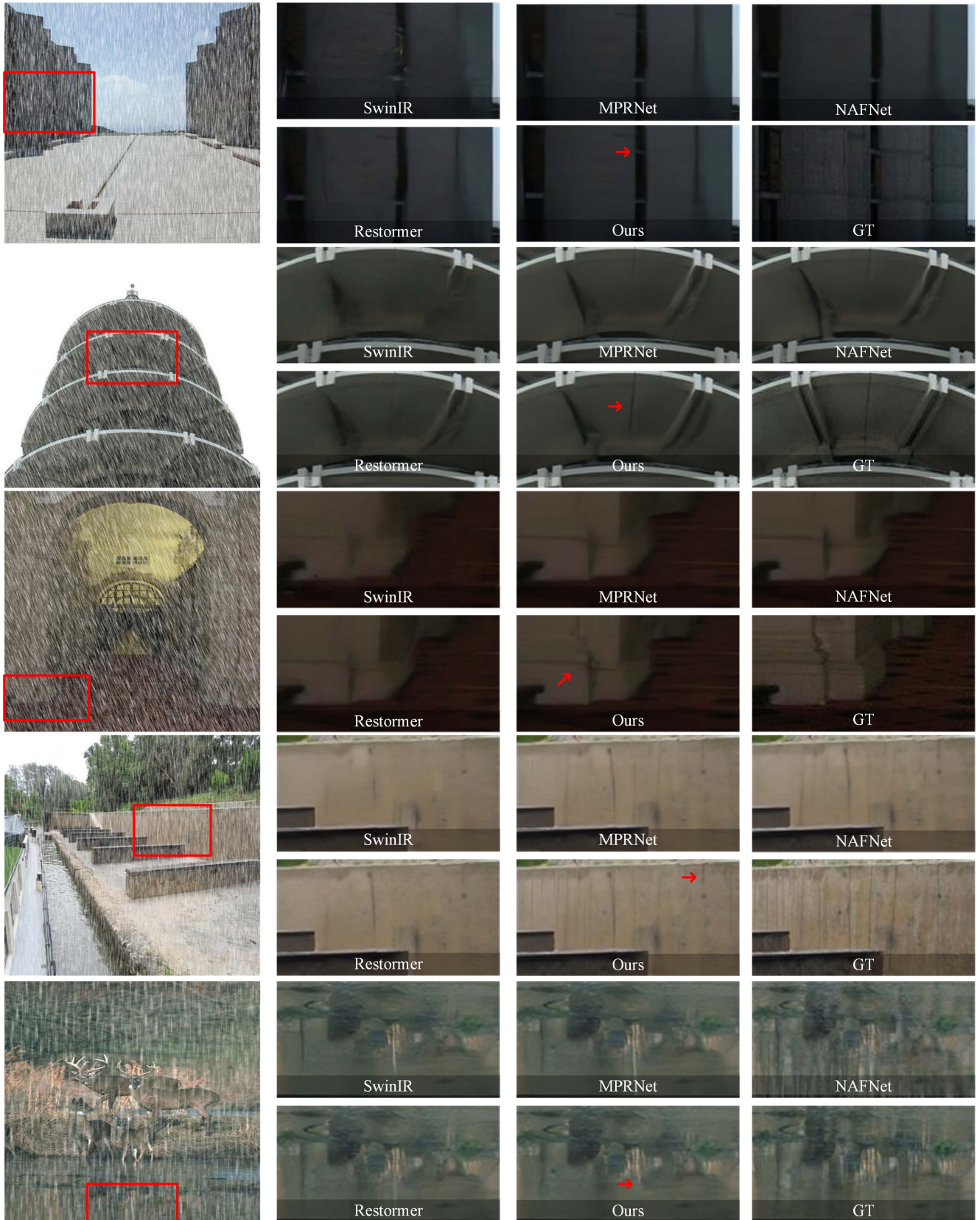


Figure I. Visual comparison of results with specific models (deraining).

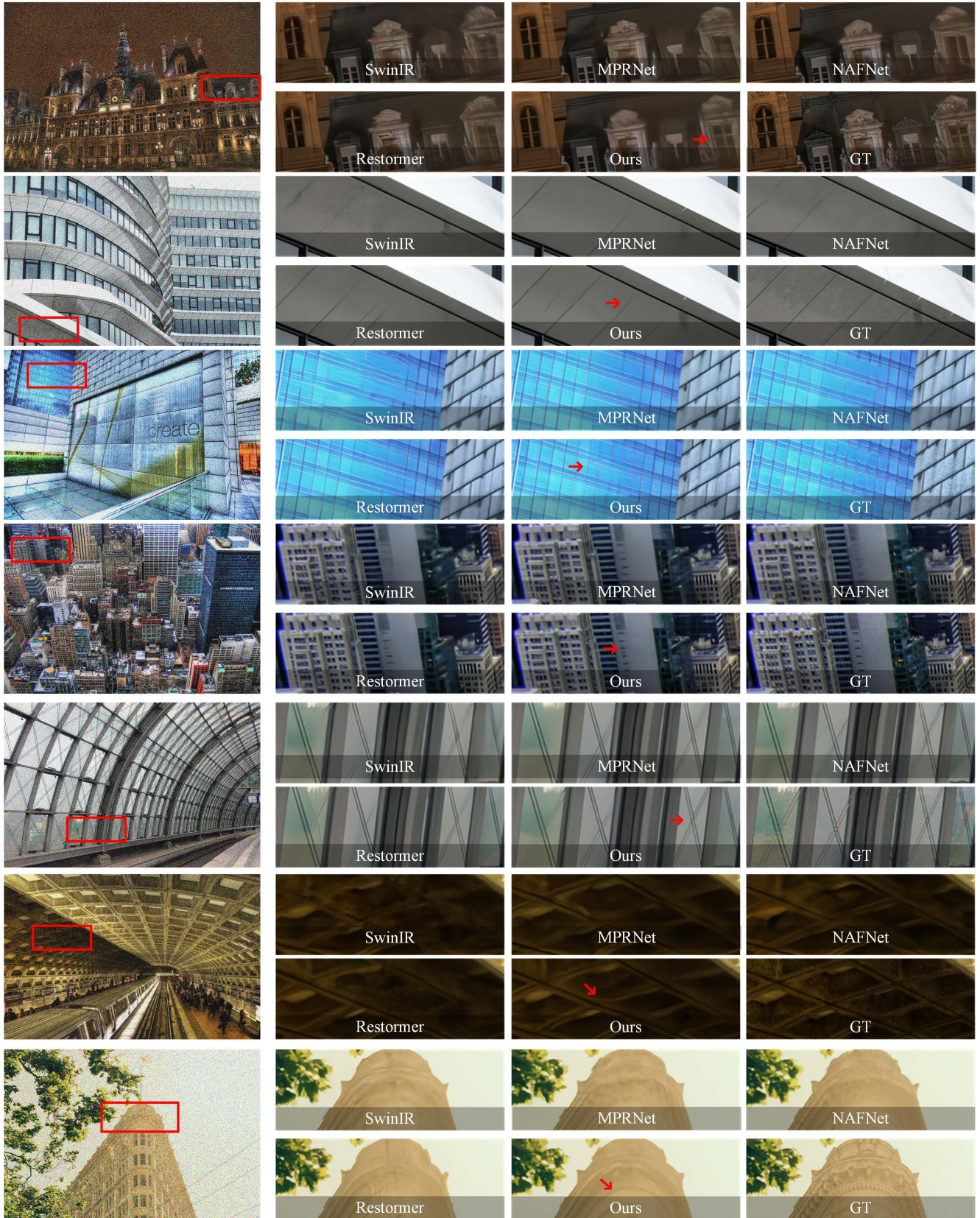


Figure J. Visual comparison of results with specific models (Gaussian-denoising).

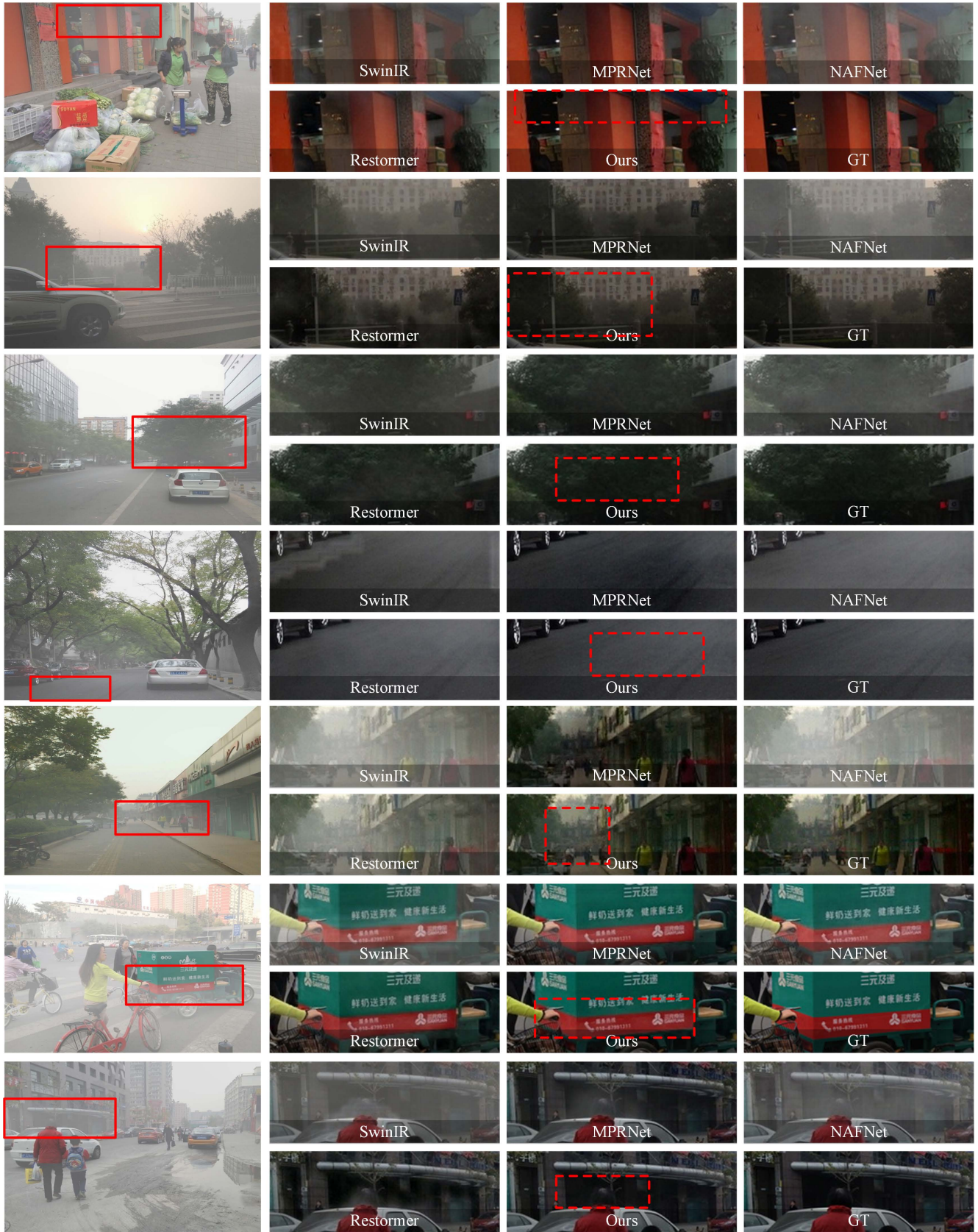


Figure K. Visual comparison of results with specific models (dehaze).

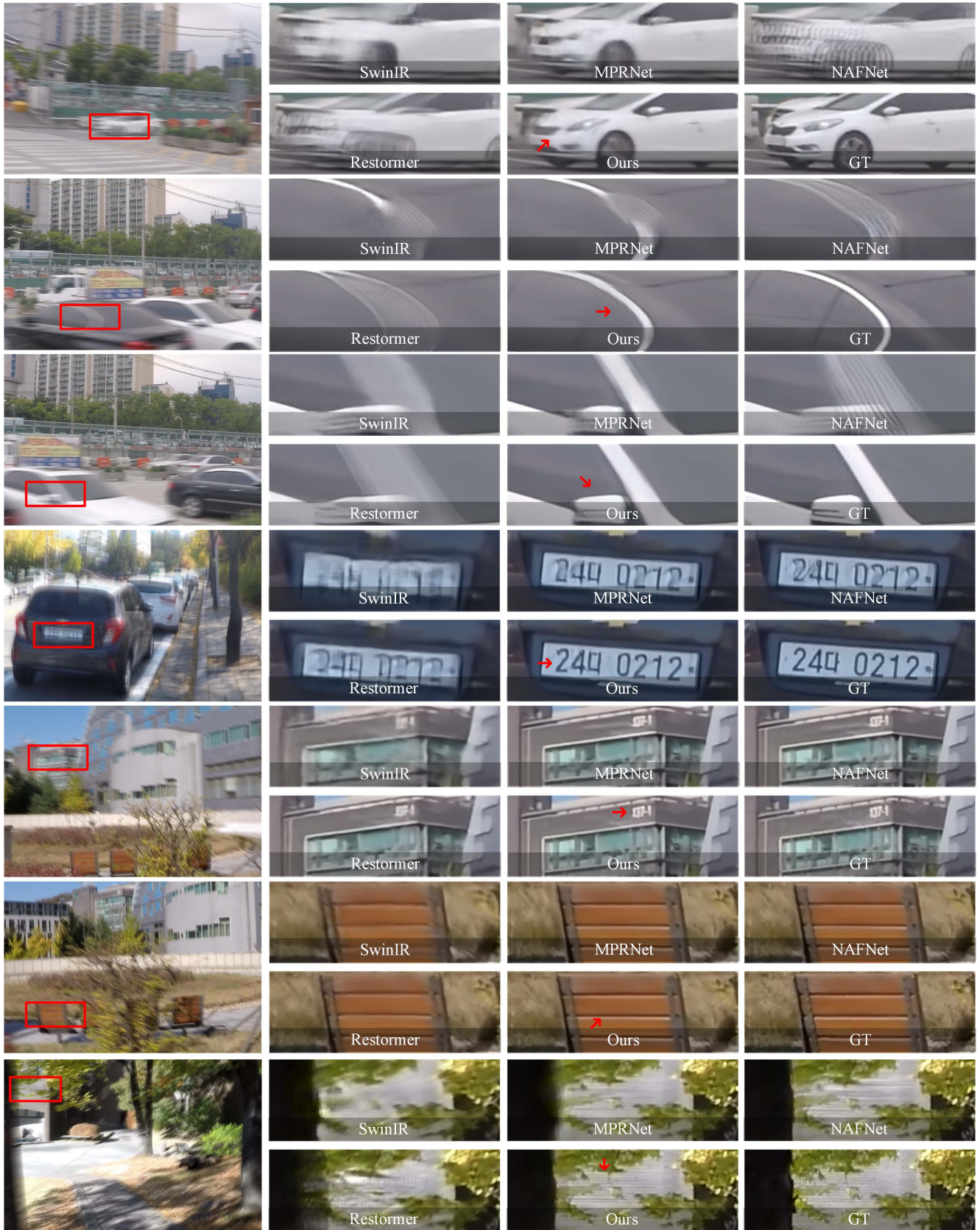


Figure L. Visual comparison of results with specific models (motion-deblurring).



Figure M. Visual comparison of results with specific models (desnowing).

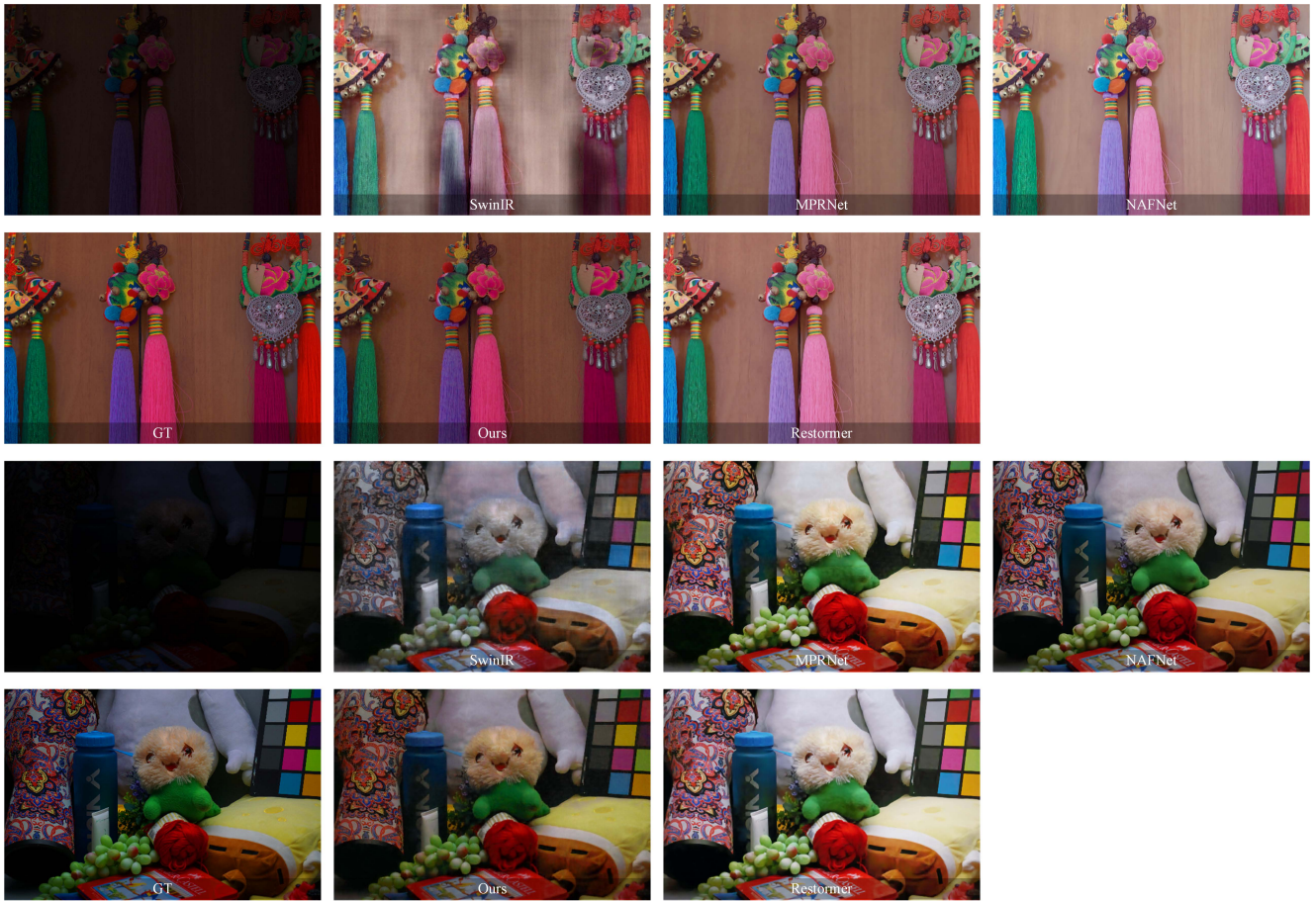


Figure N. Visual comparison of results with specific models (lowlight enhancement).



Figure O. Visual comparison of results on All-in-One image restoration (mixed-degradation, *in-dist*). Zoom in for more details.

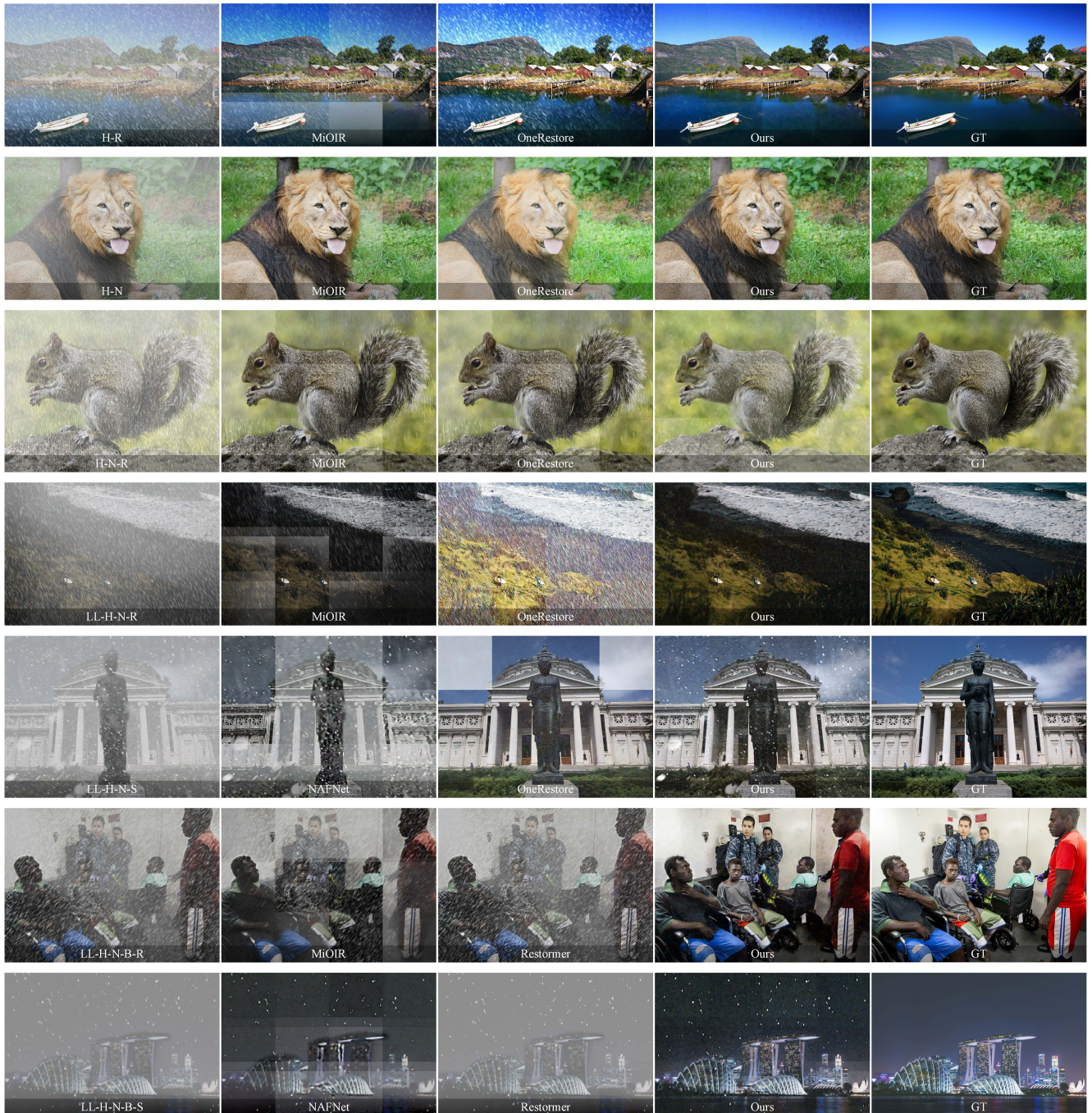


Figure P. Visual comparison of results on All-in-One image restoration (mixed-degradation, *out-dist*). Zoom in for more details.

References

- [1] Abdelrahman Abdelhamed, Stephen Lin, and Michael S. Brown. A high-quality denoising dataset for smartphone cameras. In *CVPR*, 2018. 1
- [2] Eirikur Agustsson and Radu Timofte. Ntire 2017 challenge on single image super-resolution: Dataset and study. In *CVPRW*, 2017. 1
- [3] Yuang Ai, Huaibo Huang, and Ran He. Lora-ir: Taming low-rank experts for efficient all-in-one image restoration. *arXiv preprint arXiv:2410.15385*, 2024. 1
- [4] Yuang Ai, Huaibo Huang, and Ran He. Lora-ir: Taming low-rank experts for efficient all-in-one image restoration. *arXiv preprint arXiv:2410.15385*, 2024. 3, 2
- [5] Yuang Ai, Huaibo Huang, Xiaoqiang Zhou, Jiexiang Wang, and Ran He. Multimodal prompt perceiver: Empower adaptiveness, generalizability and fidelity for all-in-one image restoration. In *CVPR*, 2024. 1, 3
- [6] FirstName Alpher. Frobnication. *IEEE TPAMI*, 12(1):234–778, 2002.
- [7] FirstName Alpher and FirstName Fotheringham-Smythe. Frobnication revisited. *Journal of Foo*, 13(1):234–778, 2003.
- [8] FirstName Alpher and FirstName Gamow. Can a computer frobnicate? In *CVPR*, pages 234–778, 2005.
- [9] FirstName Alpher, FirstName Fotheringham-Smythe, and FirstName Gamow. Can a machine frobnicate? *Journal of Foo*, 14(1):234–778, 2004.
- [10] Lester Brian, Al-Rfou Rami, and Constant Noah. The power of scale for parameter-efficient prompt tuning. In *EMNLP*, 2021. 1, 3
- [11] Yuanhao Cai, Hao Bian, Jing Lin, Haoqian Wang, Radu Timofte, and Yulun Zhang. Retinexformer: One-stage retinex-based transformer for low-light image enhancement. In *ICCV*, 2023. 2
- [12] Jin Cao, Yi Cao, Li Pang, Deyu Meng, and Xiaoyong Cao. Hair: Hypernetworks-based all-in-one image restoration. *arXiv preprint arXiv:2408.08091*, 2024. 1, 3
- [13] Shuo Cao, Yihao Liu, Wenlong Zhang, Yu Qiao, and Chao Dong. Grids: Grouped multiple-degradation restoration with image degradation similarity. In *ECCV*, 2024. 1, 3, 2
- [14] Jie Chang, Zhonghao Lan, Changmao Cheng, and Yichen Wei. Data uncertainty learning in face recognition. In *CVPR*, 2020. 5
- [15] Haoyu Chen, Wenbo Li, Jinjin Gu, Jingjing Ren, Sixiang Chen, Tian Ye, Renjing Pei, Kaiwen Zhou, Fenglong Song, and Lei Zhu. Restoagent: Autonomous image restoration agent via multimodal large language models. In *NeurIPS*, 2024. 1, 3, 6, 2
- [16] Liangyu Chen, Xiaojie Chu, Xiangyu Zhang, and Jian Sun. Simple baselines for image restoration. In *ECCV*, 2022. 1, 3, 6, 7, 8, 4
- [17] Zitian Chen, Mingyu Ding, Yikang Shen, Wei Zhan, Masayoshi Tomizuka, Erik Learned-Miller, and Chuang Gan. An efficient general-purpose modular vision model via multi-task heterogeneous training. *arXiv preprint arXiv:2306.17165*, 2023. 3
- [18] Zitian Chen, Yikang Shen, Mingyu Ding, Zhenfang Chen, Hengshuang Zhao, Erik Learned-Miller, and Chuang Gan. Mod-squad: Designing mixtures of experts as modular multi-task learners. *CVPR*, 2023. 3
- [19] Aidan Clark, Diego de las Casas, Aurelia Guy, Arthur Mensch, Michela Paganini, Jordan Hoffmann, Bogdan Damoc, Blake Hechtman, Trevor Cai, Sebastian Borgeaud, George van den Driessche, Eliza Rutherford, Tom Hennigan, Matthew Johnson, Katie Millican, Albin Cassirer, Chris Jones, Elena Buchatskaya, David Budden, Laurent Sifre, Simon Osindero, Oriol Vinyals, Jack Rae, Erich Elsen, Koray Kavukcuoglu, and Karen Simonyan. Unified scaling laws for routed language models. In *NeurIPS*, 2022.
- [20] Marcos V. Conde, Gregor Geigle, and Radu Timofte. Instructir: High-quality image restoration following human instructions. In *ECCV*, 2024. 1, 3, 6, 8
- [21] Chao Dong, Chen Change Loy, Kaiming He, and Xiaoou Tang. Learning a deep convolutional network for image super-resolution. In *ECCV*, 2014. 1, 3
- [22] Qingnan Fan, Dongdong Chen, Lu Yuan, Gang Hua, Nenghai Yu, and Baoquan Chen. A general decoupled learning framework for parameterized image operators. *IEEE TPAMI*, 2019. 6
- [23] William Fedus, Barret Zoph, and Noam Shazeer. Switch transformers: Scaling to trillion parameter models with simple and efficient sparsity. *Journal of Machine Learning Research*, 2022. 3
- [24] Xueyang Fu, Jiabin Huang, Delu Zeng, Yue Huang, Xinghao Ding, and John Paisley. Removing rain from single images via a deep detail network. In *CVPR*, 2017. 1, 7
- [25] Yun Guo, Xueyao Xiao, Yi Chang, Shumin Deng, and Luxin Yan. From sky to the ground: A large-scale benchmark and simple baseline towards real rain removal. In *ICCV*, 2023. 5, 8
- [26] Yu Guo, Yuan Gao, Yuxu Lu, Ryan Wen Liu, and Shengfeng He. Onerestore: A universal restoration framework for composite degradation. In *ECCV*, 2024. 1, 6, 8, 2, 3, 4
- [27] Jingwen He, Chao Dong, and Yu Qiao. Modulating image restoration with continual levels via adaptive feature modification layers. In *The IEEE Conference on Computer Vision and Pattern Recognition (CVPR)*, 2019.
- [28] Kaiming He, Xiangyu Zhang, Shaoqing Ren, and Jian Sun. Deep residual learning for image recognition. In *CVPR*, 2016. 1
- [29] Neil Houlsby, Andrei Giurgiu, Stanislaw Jastrzebski, Bruna Morrone, Quentin de Laroussilhe, Andrea Gesmundo, Mona Attariyan, and Sylvain Gelly. Parameter-efficient transfer learning for nlp. In *ICML*, 2019. 1, 3
- [30] Edward J Hu, Yelong Shen, Phillip Wallis, Zeyuan Allen-Zhu, Yuanzhi Li, Shean Wang, Lu Wang, and Weizhu Chen. LoRA: Low-rank adaptation of large language models. In *ICLR*, 2022.
- [31] Robert A. Jacobs, Michael I. Jordan, Steven J. Nowlan, and Geoffrey E. Hinton. Adaptive mixtures of local experts. *Neural Computation*, 1991.

- [32] Junjun Jiang, Zengyuan Zuo, Gang Wu, Kui Jiang, and Xianming Liu. A survey on all-in-one image restoration: Taxonomy, evaluation and future trends. *arXiv preprint arXiv:2410.15067*, 2024. 1
- [33] M.I. Jordan and R.A. Jacobs. Hierarchical mixtures of experts and the em algorithm. In *Proceedings of 1993 International Conference on Neural Networks (IJCNN-93-Nagoya, Japan)*, 1993.
- [34] Orest Kupyn, Tetiana Martyniuk, Junru Wu, and Zhangyang Wang. Deblurgan-v2: Deblurring (orders-of-magnitude) faster and better. In *ICCV*, 2019. 1, 3
- [35] FirstName LastName. The frobnicatable foo filter, 2014. Face and Gesture submission ID 324. Supplied as supplemental material fg324.pdf.
- [36] FirstName LastName. Frobnication tutorial, 2014. Supplied as supplemental material tr.pdf.
- [37] Dmitry Lepikhin, HyoukJoong Lee, Yuanzhong Xu, Dehao Chen, Orhan Firat, Yanping Huang, Maxim Krikun, Noam Shazeer, and Zhifeng Chen. {GS}hard: Scaling giant models with conditional computation and automatic sharding. In *ICLR*, 2021. 3
- [38] Mike Lewis, Shruti Bhosale, Tim Dettmers, Naman Goyal, and Luke Zettlemoyer. Base layers: Simplifying training of large, sparse models. In *NeurIPS*, 2021.
- [39] Boyi Li, Wenqi Ren, Dengpan Fu, Dacheng Tao, Dan Feng, Wenjun Zeng, and Zhangyang Wang. Benchmarking single-image dehazing and beyond. *IEEE TIP*, 28(1): 492–505, 2019. 6, 7, 1
- [40] Boyun Li, Xiao Liu, Peng Hu, Zhongqin Wu, Jiancheng Lv, and Xi Peng. All-In-One Image Restoration for Unknown Corruption. In *CVPR*, 2022. 1, 3, 6
- [41] Chongyi Li, Chunle Guo, Wenqi Ren, Runmin Cong, Junhui Hou, Sam Kwong, and Dacheng Tao. An underwater image enhancement benchmark dataset and beyond. *IEEE TIP*, 29:4376–4389, 2020. 5, 4
- [42] Hao Li, Xiang Chen, Jiangxin Dong, Jinhui Tang, and Jinshan Pan. Foundir: Unleashing million-scale training data to advance foundation models for image restoration. *arXiv preprint arXiv:2412.01427*, 2024.
- [43] Junnan Li, Dongxu Li, Caiming Xiong, and Steven C. H. Hoi. BLIP: bootstrapping language-image pre-training for unified vision-language understanding and generation. In *ICML*, 2022. 4
- [44] Junnan Li, Dongxu Li, Silvio Savarese, and Steven C. H. Hoi. BLIP-2: bootstrapping language-image pre-training with frozen image encoders and large language models. In *ICML*, 2023. 4
- [45] Junyi Li, Zhilu Zhang, Xiaoyu Liu, Chaoyu Feng, Xiaotao Wang, Lei Lei, and Wangmeng Zuo. Spatially adaptive self-supervised learning for real-world image denoising. In *CVPR*, 2023.
- [46] Junyi Li, Zhilu Zhang, and Wangmeng Zuo. Tbsn: Transformer-based blind-spot network for self-supervised image denoising. *arXiv preprint arXiv:2404.07846*, 2024.
- [47] Youwei Li, Haibin Huang, Lanpeng Jia, Haoqiang Fan, and Shuaicheng Liu. D2c-sr: A divergence to convergence approach for real-world image super-resolution. In *ECCV*, 2022. 1
- [48] Jingyun Liang, Jiezhong Cao, Guolei Sun, Kai Zhang, Luc Van Gool, and Radu Timofte. Swinir: Image restoration using swin transformer. In *ICCV*, 2021. 1, 3, 6, 7, 8
- [49] Jie Liang, Hui Zeng, and Lei Zhang. Efficient and degradation-adaptive network for real-world image super-resolution. In *ECCV*, 2022. 1
- [50] Bee Lim, Sanghyun Son, Heewon Kim, Seungjun Nah, and Kyoung Mu Lee. Enhanced deep residual networks for single image super-resolution. In *CVPRW*, 2017. 1
- [51] Jingbo Lin, Zhilu Zhang, Yuxiang Wei, Dongwei Ren, Dongsheng Jiang, Qi Tian, and Wangmeng Zuo. Improving image restoration through removing degradations in textual representations. In *CVPR*, 2024. 1
- [52] Lin Liu, Lingxi Xie, Xiaopeng Zhang, Shanxin Yuan, Xiangyu Chen, Wengang Zhou, Houqiang Li, and Qi Tian. Tape: Task-agnostic prior embedding for image restoration. In *ECCV*, 2022. 6
- [53] Xiaohui Liu, Zhilu Zhang, Xiaohe Wu, Chaoyu Feng, Xiaotao Wang, Lei Lei, and Wangmeng Zuo. Learning real-world image de-weathering with imperfect supervision. In *AAAI*, 2024. 1
- [54] Yihao Liu, Anran Liu, Jinjin Gu, Zhipeng Zhang, Wenhao Wu, Yu Qiao, and Chao Dong. Discovering distinctive “semantics” in super-resolution networks. *arXiv preprint arXiv:2108.00406*, 2022. 8
- [55] Yihao Liu, Jingwen He, Jinjin Gu, Xiangtao Kong, Yu Qiao, and Chao Dong. Degae: A new pretraining paradigm for low-level vision. In *CVPR*, 2023.
- [56] Yun-Fu Liu, Da-Wei Jaw, Shih-Chia Huang, and Jenq-Neng Hwang. Desnownet: Context-aware deep network for snow removal. *IEEE TIP*, 27(6):3064–3073, 2018.
- [57] Yun-Fu Liu, Da-Wei Jaw, Shih-Chia Huang, and Jenq-Neng Hwang. Desnownet: Context-aware deep network for snow removal. *IEEE TIP*, 27(6):3064–3073, 2018. 1, 5, 6, 7, 2
- [58] Ze Liu, Yutong Lin, Yue Cao, Han Hu, Yixuan Wei, Zheng Zhang, Stephen Lin, and Baining Guo. Swin transformer: Hierarchical vision transformer using shifted windows. In *ICCV*, 2021. 1
- [59] Ziwei Luo, Fredrik K Gustafsson, Zheng Zhao, Jens Sjölund, and Thomas B Schön. Controlling vision-language models for universal image restoration. In *ICLR*, 2024. 4, 8
- [60] Kede Ma, Zhengfang Duanmu, Qingbo Wu, Zhou Wang, Hongwei Yong, Hongliang Li, and Lei Zhang. Waterloo exploration database: New challenges for image quality assessment models. *IEEE Transactions on Image Processing*, 2017. 1
- [61] David R. Martin, Charless C. Fowlkes, Doron Tal, and Jitendra Malik. A database of human segmented natural images and its application to evaluating segmentation algorithms and measuring ecological statistics. In *ICCV*, 2001. 6, 7, 1
- [62] Tom M Mitchell. *Machine learning*. 1997. 4
- [63] Basil Mustafa, Carlos Riquelme Ruiz, Joan Puigcerver, Rodolphe Jenatton, and Neil Houlsby. Multimodal contrastive learning with LIMoe: the language-image mixture of experts. In *NeurIPS*, 2022.

- [64] Seungjun Nah, Tae Hyun Kim, and Kyoung Mu Lee. Deep multi-scale convolutional neural network for dynamic scene deblurring. In *CVPR*, 2017. 1, 6, 7
- [65] Seungjun Nah, Tae Hyun Kim, and Kyoung Mu Lee. Deep multi-scale convolutional neural network for dynamic scene deblurring. In *CVPR*, 2017. 1
- [66] Dongwon Park, Byung Hyun Lee, and Se Young Chun. All-in-one image restoration for unknown degradations using adaptive discriminative filters for specific degradations. In *CVPR*, 2023. 1, 3, 2
- [67] Vaishnav Potlapalli, Syed Waqas Zamir, Salman Khan, and Fahad Khan. Promptir: Prompting for all-in-one image restoration. In *NeurIPS*, 2023. 1, 3, 6, 7, 8, 4
- [68] Joan Puigcerver, Carlos Riquelme Ruiz, Basil Mustafa, and Neil Houlsby. From sparse to soft mixtures of experts. In *ICLR*, 2024. 3
- [69] Rui Qian, Robby T. Tan, Wenhan Yang, Jiajun Su, and Jiaying Liu. Attentive generative adversarial network for rain-drop removal from a single image. In *CVPR*, 2018. 5, 4
- [70] Alec Radford, Jong Wook Kim, Chris Hallacy, Aditya Ramesh, Gabriel Goh, Sandhini Agarwal, Girish Sastry, Amanda Askell, Pamela Mishkin, Jack Clark, Gretchen Krueger, and Ilya Sutskever. Learning transferable visual models from natural language supervision. In *ICML*, 2021. 1
- [71] Samyam Rajbhandari, Conglong Li, Zhewei Yao, Minjia Zhang, Reza Yazdani Aminabadi, Ammar Ahmad Awan, Jeff Rasley, and Yuxiong He. Deepspeed-moe: Advancing mixture-of-experts inference and training to power next-generation ai scale. In *ICML*, 2022. 3
- [72] Dongwei Ren, Wangmeng Zuo, Qinghua Hu, Pengfei Zhu, and Deyu Meng. Progressive image deraining networks: A better and simpler baseline. In *CVPR*, 2019. 1, 3
- [73] Jaesung Rim, Haeyun Lee, Jucheol Won, and Sunghyun Cho. Real-world blur dataset for learning and benchmarking deblurring algorithms. In *ECCV*, 2020. 1
- [74] Carlos Riquelme Ruiz, Joan Puigcerver, Basil Mustafa, Maxim Neumann, Rodolphe Jenatton, André Susano Pinto, Daniel Keysers, and Neil Houlsby. Scaling vision with sparse mixture of experts. In *Advances in Neural Information Processing Systems*, 2021.
- [75] Noam Shazeer, *Azalia Mirhoseini, *Krzysztof Maziarz, Andy Davis, Quoc Le, Geoffrey Hinton, and Jeff Dean. Outrageously large neural networks: The sparsely-gated mixture-of-experts layer. In *ICLR*, 2017. 3, 5
- [76] H.R. Sheikh, Z.Wang, L. Cormack, and A.C. Bovik. Live image quality assessment database release 2. <http://live.ece.utexas.edu/research/quality>. 6, 7, 1
- [77] Sheng Shen, Zhewei Yao, Chunyuan Li, Trevor Darrell, Kurt Keutzer, and Yuxiong He. Scaling vision-language models with sparse mixture of experts. In *EMNLP*, 2023.
- [78] Karen Simonyan and Andrew Zisserman. Very deep convolutional networks for large-scale image recognition. In *ICLR*, 2015. 8
- [79] Yuda Song, Zhuqing He, Hui Qian, and Xin Du. Vision transformers for single image dehazing. *IEEE TIP*, 32: 1927–1941, 2023. 1, 3
- [80] Yujing Sun, Yizhou Yu, and Wenping Wang. Moiré photo restoration using multiresolution convolutional neural networks. *IEEE TIP*, 27(8):4160–4172, 2018.
- [81] Yuchuan Tian, Jianhong Han, Hanting Chen, Yuanyuan Xi, Guoyang Zhang, Jie Hu, Chao Xu, and Yunhe Wang. Instruct-ipt: All-in-one image processing transformer via weight modulation. *arXiv preprint arXiv:2407.00676*, 2024. 1, 3, 2
- [82] Jeya Maria Jose Valanarasu, Rajevee Yasarla, and Vishal M. Patel. Transweather: Transformer-based restoration of images degraded by adverse weather conditions. In *CVPR*, 2022. 1, 3, 6
- [83] Ashish Vaswani, Noam Shazeer, Niki Parmar, Jakob Uszkoreit, Llion Jones, Aidan N Gomez, Łukasz Kaiser, and Illia Polosukhin. Attention is all you need. In *NeurIPS*, 2017. 1
- [84] Feng Wang, Jian Cheng, Weiyang Liu, and Haijun Liu. Additive margin softmax for face verification. *IEEE Signal Processing Letters*, 2018.
- [85] Xintao Wang, Liangbin Xie, Chao Dong, and Ying Shan. Real-esrgan: Training real-world blind super-resolution with pure synthetic data. In *ICCVW*, 2021. 1, 4
- [86] Chen Wei, Wenjing Wang, Wenhan Yang, and Jiaying Liu. Deep retinex decomposition for low-light enhancement. In *BMVC*, 2018. 1, 6, 7
- [87] Zhang Wenlong, Li Xiaohui, Guangyuan SHI, Chen Xiangyu, Qiao Yu, Zhang Xiaoyun, Wu Xiao-Ming, and Dong Chao. Real-world image super-resolution as multi-task learning. In *NeurIPS*, 2023. 1, 3
- [88] Lemeng Wu, Mengchen Liu, Yinpeng Chen, Dongdong Chen, Xiyang Dai, and Lu Yuan. Residual mixture of experts. *arXiv preprint arXiv:2204.09636*, 2022.
- [89] Xun Wu, Shaohan Huang, and Furu Wei. Mixture of loRA experts. In *ICLR*, 2024.
- [90] Kong Xiangtao, Dong Chao, and Zhang Lei. Towards effective multiple-in-one image restoration: A sequential and prompt learning strategy. *arXiv preprint arXiv:2401.03379*, 2024. 1, 3, 6, 8, 4
- [91] Liangbin Xie, Xintao Wang, Chao Dong, Zhongang Qi, and Ying Shan. Finding discriminative filters for specific degradations in blind super-resolution. In *NeurIPS*, 2021.
- [92] Xiaogang Xu, Ruixing Wang, Chi-Wing Fu, , and Jiaya Jia. Snr-aware low-light image enhancement. In *CVPR*, 2022. 1, 5, 8
- [93] Yimin Xu, Nanxi Gao, Yunshan Zhong, Fei Chao, and Rongrong Ji. Unified-width adaptive dynamic network for all-in-one image restoration. *arXiv preprint arXiv:2405.15475*, 2024. 1, 3
- [94] Qinhong Yang, Dongdong Chen, Zhentao Tan, Qiankun Liu, Qi Chu, Jianmin Bao, Lu Yuan, Gang Hua, and Nenghai Yu. Hq-50k: A large-scale, high-quality dataset for image restoration. *arXiv preprint arXiv:2306.05390*, 2023. 1, 3
- [95] Wenhan Yang, Robby T. Tan, Jiashi Feng, Jiaying Liu, Zongming Guo, and Shuicheng Yan. Deep joint rain detection and removal from a single image. In *CVPR*, 2017. 6, 7, 1, 4

- [96] Eduard Zamfir, Zongwei Wu, Nancy Mehta, Danda Dani Paudel, Yulun Zhang, and Radu Timofte. Efficient degradation-aware any image restoration. *arXiv preprint arXiv:2405.15475*, 2024. 3
- [97] Syed Waqas Zamir, Aditya Arora, Salman Khan, Munawar Hayat, Fahad Shahbaz Khan, Ming-Hsuan Yang, and Ling Shao. Multi-stage progressive image restoration. In *CVPR*, 2021. 1, 3, 6, 7, 8
- [98] Syed Waqas Zamir, Aditya Arora, Salman Khan, Munawar Hayat, Fahad Shahbaz Khan, and Ming-Hsuan Yang. Restormer: Efficient transformer for high-resolution image restoration. In *CVPR*, 2022. 1, 3, 6, 7, 8, 2, 4
- [99] He Zhang and Vishal M. Patel. Density-aware single image de-raining using a multi-stream dense network. In *CVPR*, 2018. 1, 7
- [100] Jinghao Zhang, Jie Huang, Mingde Yao, Zizheng Yang, Hu Yu, Man Zhou, and Feng Zhao. Ingredient-oriented multi-degradation learning for image restoration. In *CVPR*, 2023. 1, 3, 6
- [101] Kai Zhang, Wangmeng Zuo, Yunjin Chen, Deyu Meng, and Lei Zhang. Beyond a gaussian denoiser: Residual learning of deep CNN for image denoising. *IEEE TIP*, 26(7):3142–3155, 2017. 1, 3
- [102] Kai Zhang, Wangmeng Zuo, and Lei Zhang. Learning a single convolutional super-resolution network for multiple degradations. In *CVPR*, 2018. 3, 1
- [103] Kai Zhang, Jingyun Liang, Luc Van Gool, and Radu Timofte. Designing a practical degradation model for deep blind image super-resolution. In *ICCV*, 2021. 1
- [104] Lei Zhang, Xiaolin Wu, Antoni Buades, and Xin Li. Color demosaicking by local directional interpolation and non-local adaptive thresholding. *J. Electronic Imaging*, 20(2):023016, 2011.
- [105] Ruofan Zhang, Jinjin Gu, Haoyu Chen, Chao Dong, Yulun Zhang, and Wenming Yang. Crafting training degradation distribution for the accuracy-generalization trade-off in real-world super-resolution. In *ICML*, 2023.
- [106] Wenlong Zhang, Guangyuan Shi, Yihao Liu, Chao Dong, and Xiao-Ming Wu. A closer look at blind super-resolution: Degradation models, baselines, and performance upper bounds. In *CVPRW*, 2022. 1
- [107] Xinyi Zhang, Hang Dong, Jinshan Pan, Chao Zhu, Ying Tai, Chengjie Wang, Jilin Li, Feiyue Huang, and Fei Wang. Learning to restore hazy video: A new real-world dataset and a new method. In *CVPR*, pages 9239–9248, 2021.
- [108] Yabo Zhang, Yuxiang Wei, Dongsheng Jiang, Xiaopeng Zhang, Wangmeng Zuo, and Qi Tian. Controlvideo: Training-free controllable text-to-video generation. *arXiv preprint arXiv:2305.13077*, 2023. 1
- [109] Zhilu Zhang, Haolin Wang, Ming Liu, Ruohao Wang, Jiawei Zhang, and Wangmeng Zuo. Learning raw-to-srgb mappings with inaccurately aligned supervision. In *ICCV*, 2021. 1
- [110] Zhilu Zhang, RongJian Xu, Ming Liu, Zifei Yan, and Wangmeng Zuo. Self-supervised image restoration with blurry and noisy pairs. In *NeurIPS*, 2022. 1
- [111] Zhilu Zhang, Shuohao Zhang, Renlong Wu, Zifei Yan, and Wangmeng Zuo. Bracketing is all you need: Unifying image restoration and enhancement tasks with multi-exposure images. *arXiv preprint arXiv:2401.00766*, 2024. 1
- [112] Zihan Zhong, Zhiqiang Tang, Tong He, Haoyang Fang, and Chun Yuan. Convolution meets loRA: Parameter efficient finetuning for segment anything model. In *ICLR*, 2024.
- [113] Yuqian Zhou, David Ren, Neil Emerton, Sehoon Lim, and Timothy Large. Image restoration for under-display camera. In *CVPR*, 2021. 5, 4
- [114] Jinguo Zhu, Xizhou Zhu, Wenhai Wang, Xiaohua Wang, Hongsheng Li, Xiaogang Wang, and Jifeng Dai. Uni-perceiver-moe: Learning sparse generalist models with conditional moes. In *NeurIPS*, 2022. 3
- [115] Yurui Zhu, Tianyu Wang, Xueyang Fu, Xuanyu Yang, Xin Guo, Jifeng Dai, Yu Qiao, and Xiaowei Hu. Learning weather-general and weather-specific features for image restoration under multiple adverse weather conditions. In *CVPR*, 2023. 1, 3, 8, 2
- [116] Barret Zoph, Irwan Bello, Sameer Kumar, Nan Du, Yanping Huang, Jeff Dean, Noam Shazeer, and William Fedus. St-moe: Design stable and transferable sparse expert models. *arXiv preprint arXiv:2202.08906*, 2022. 3